IOPscience iopscience.iop.org

Home Search Collections Journals About Contact us My IOPscience

Epitaxial patterning of thin-films: conventional lithographies and beyond

This content has been downloaded from IOPscience. Please scroll down to see the full text.

2014 J. Micromech. Microeng. 24 093001

(http://iopscience.iop.org/0960-1317/24/9/093001)

View the table of contents for this issue, or go to the journal homepage for more

Download details:

IP Address: 205.175.116.127
This content was downloaded on 05/08/2014 at 22:26

Please note that terms and conditions apply.

IOP Publishing Journal of Micromechanics and Microengineering
J. Micromech. Microeng. **24** (2014) 093001 (23pp) doi:10.1088/0960-1317/24/9/093001

Topical Review

Epitaxial patterning of thin-films: conventional lithographies and beyond

Wei Zhang[1,2] **and Kannan M Krishnan**[1]

[1] Department of Materials Science and Engineering, University of Washington, Seattle, WA, 98195, USA

E-mail: zwei@anl.gov and kannanmk@uw.edu

Received 14 April 2014
Accepted for publication 29 May 2014
Published 31 July 2014

Abstract

Thin-film based novel magnetic and electronic devices have entered a new era in which the film crystallography, structural coherence, and epitaxy play important roles in determining their functional properties. The capabilities of controlling such structural and functional properties are being continuously developed by various physical deposition technologies. Epitaxial patterning strategies further allow the miniaturization of such novel devices, which incorporates thin-film components into nanoscale architectures while keeping their functional properties unmodified from their ideal single-crystal values. In the past decade, epitaxial patterning methods on the laboratory scale have been reported to meet distinct scientific inquires, in which the techniques and processes used differ from one to the other. In this review we summarize many of these pioneering endeavors in epitaxial patterning of thin-film devices that use both conventional and novel lithography techniques. These methods demonstrate epitaxial patterning for a broad range of materials (metals, oxides, and semiconductors) and cover common device length scales from micrometer to sub-hundred nanometer. Whilst we have been motivated by magnetic materials and devices, we present our outlook on developing systematic-strategies for epitaxial patterning of functional materials which will pave the road for the design, discovery and industrialization of next-generation advanced magnetic and electronic nano-devices.

Keywords: epitaxial patterning, magnetic thin films, nanoimprint lithography, nanomagnetism

(Some figures may appear in colour only in the online journal)

1. Introduction and background

Epitaxial ferromagnetic, ferroelectric, and multiferroic thin films are of crucial importance to modern and future spin-electronic devices [1–3]. These thin films, usually made of metals and oxides, are preferably fabricated by robust physical deposition methods (figure 1(*a*)), including magnetron sputtering, ion beam sputtering (IBS), pulsed laser deposition (PLD), and molecular beam epitaxy (MBE). In order to achieve epitaxial growth of these thin films, the host substrates are usually polished single crystals cleaved along certain orientations, having minimum lattice mismatch with the material to be deposited. The deposition process also needs to be critically controlled, which usually takes place in a vacuum chamber with a base pressure ranging from 10^{-7} to 10^{-10} Torr, in order to guarantee a clean surface and high purity of the deposited thin films. The substrates are also heated to elevated temperatures during deposition, providing enough mobility to the arriving material adatoms to rearrange themselves on the substrate. The deposition rate is typically very low level, usually less than 1 Å/s. The high substrate temperature and the low deposition rate provide sufficient energy and time for the adsorbed species to move around and reach their lowest energy state, duplicating the crystal lattice structure

[2] Present address: Materials Science Division, Argonne National Laboratory, Argonne, IL , USA

 © 2014 IOP Publishing Ltd Printed in the UK

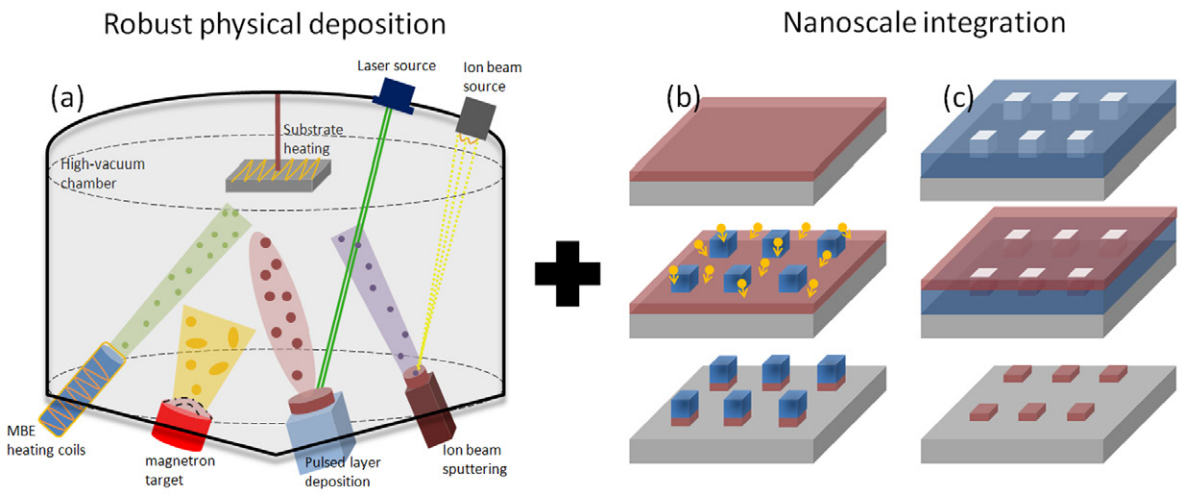

Figure 1. (*a*) Thin film fabrication via robust physical deposition methods. Schematic illustration of nanoscale integration via either (*b*) deposition → lithography → post-etching or (*c*) lithography →deposition → liftoff processes.

(homoepitaxy) and/or matching the crystalline order of the substrate (heteroepitaxy). Depending on the free energies of the surface and interface, different growth modes, i.e. layer by layer, Stranski-Krastanov, and island growth, can be achieved with distinct film morphologies and properties. With well-controlled growth recipes, epitaxial growth can place stringent demands on a deposited layer and also create clean surface for device fabrication. Advantages of epitaxial thin films include high purity, low defect, abrupt interfaces, high repeatability and high uniformity.

Recently, there is also an increasing demand for fabricating epitaxial thin films in the nanostructured form, to miniaturize integrated devices and extend the potential of establishing full nanoscale architectures [4]. Top-down lithography techniques, such as photolithography and electron-beam lithography (EBL), have been offering great opportunities for patterning materials into nanostructures, especially into ordered arrays. As a result, an integrated process combining lithography and direct deposition is a favorable approach for epitaxial patterning of thin-film materials. On one hand, direct deposition under the same recipe as for growing continuous films allows the desired composition, stoichiometry and properties to be well maintained in their nanostructured forms. On the other hand, lithography enables the fabrication of thin-film nanostructures with well-defined shape, dimension, and accurate positioning, which may be difficult to achieve in 'bottom-up' synthesis.

Depending on the sequence of deposition and lithography, the fabrication process can be classified into two main categories, i.e. (1) deposition → lithography → post-etching, and (2) lithography → deposition → liftoff. They are schematically illustrated in figures 1(*b*) and (*c*). In the first scenario, a continuous epitaxial thin film is first deposited on the substrate; next, lithography is performed and a mask (usually made of polymer resist) is created on top of the thin film; finally, dry-etching with good directionality is applied to remove the thin film material that is not protected by the mask; such etching is performed all the way to the substrate and therefore achieves isolated elements of the thin-film structure. The post-dry-etching process usually requires specific tools plus proper plasma combinations. For 'single-digit'(usually on the order of several nm) or small-area patterning, focused-ion beam (FIB) using Ga^+ or Ar^+ beam is a good option [5]; for wafer scale patterning, on the other hand, ion-milling and/or ion-beam etching using Ar^+ plasma have to be used [6]. The post-etching method is relatively straightforward for epitaxial patterning, and has been demonstrated for various metals and oxides [7–9]. The most appealing part of this process is the unmodified thin-film deposition step. In other words, one does not need to worry about lithography before the thin film deposition. However, the process has also yielded several controversies. One of the biggest issues is the very likely ion implantation that causes the degradation of the thin films [10, 11]. Specifically, the high energy Ar^+ or Ga^+ plasma used for material etching can inject these ions into the thin film. Further, the etching process is quite aggressive and may induce interstitial or vacancy defects [12], which can further modify the film properties, e.g. causing a conducting-insulating transition [13]. In addition, many materials, especially complex oxides, may not withstand such violent post-etching. In this case, alternative processes involving non-aggressive etching must be used. The post-etching approach for epitaxial patterning is *not* the subject of this review; this method is relatively straightforward to perform as long as the etching characteristics of the desired material and the mask are known. In the second method, a mask is generated by lithography on a clean substrate in the first place, followed by thin-film deposition through the mask; then, the mask is lifted-off by a selective etchant to achieve isolated, patterned structures. This process avoids the aggressive post-dry-etching of the thin film, eliminates the related pitfalls of ion-implantation and therefore, promises to yield high-quality patterning of a broader range of materials. Actually, such schemes have been already widely applied for patterning polycrystalline thin-film structures

[14–16], and have a great potential to be expanded to epitaxial patterning. A number of attempts have been made for epitaxial patterning nanostructures using different lithography methods, which have already resulted in some pioneering recipes and processes. However, there are new challenges associated with different types of lithographies. For instance: (1) typical epitaxial growth requires single crystal substrates. Lithographies can be technically quite difficult to perform on these special substrates, depending on the mechanisms of lithography and processes involved; (2) the process requires deposition through the mask (usually made of resist) at elevated temperatures; however, the typically used organic resists, whose glass transition temperatures are only around tens of ºC, may not withstand the elevated substrate temperature required for epitaxial growth.

In this review, we will discuss epitaxial patterning methods based on the second 'lithography →deposition → liftoff' protocol, and demonstrate how the existing challenges are either solved or circumvented by modifying the relevant processes. We will first summarize recent endeavors in epitaxial patterning using photolithography and EBL. Then, we will discuss unconventional epitaxial patterning processes using atomic-force-microcopy (AFM) lithography, nanostencil lithography (NSL), nanoimprint lithography (NIL), nanoseeding assembly, and contact printing. Depending on the specific material to be patterned, different techniques may be favored for their unique capability and compatibility. We highlight the specific material and process used with each type of lithography from the reported literatures, so that the readers can easily adapt relevant processes to their own application. Finally, we realize that there are also epitaxial-patterning developments based on 'bottom-up' chemical synthesis, such as template-guided epitaxial growth, chemical solution deposition, and chemical precursor patterning [17–20]; these techniques involve different subjects and expertise, and therefore they are not included here.

2. Review of current techniques

2.1. Photolithography and electron beam lithography (EBL)

Photolithgraphy and EBL are the most widely used techniques in most scientific laboratories with established recipes for Si-wafer-based processing, but their application to epitaxial patterning may not be straightforward due to the issues related to both the substrates and the resists. First, the *e*-beam and photon sources may have different behaviors on the single crystal substrates required for epitaxial growth, for instance, whose conductivity is often not ideal (e.g. insulators) for efficient charge dissipation. The difficulty with patterning on insulating substrates using EBL is the substrate heating and charging effect. Charging produces a large electric field at the surface, which can deflect the incoming electron beam and result in pattern distortion and positioning error [21, 22]. To overcome such a problem, the most widely used anti-charging method is to coat the resist with a light metal (such as Al, Cr, Cu [23]) or a conducting polymer layer (PEDOT/PSS, AquaSAVE [24–27]) to dissipate the charge. The latter is usually favored due to its uncomplicated application and removal process. Figure 2 compares scanning electron microscopy (SEM) images of nanostructures obtained by EBL on insulating quartz substrates with and without the top discharging layer—PEDOT/PSS (poly (3,4-Etylenedioxythiophene)/poly (styrenesulfonate [24])). The characteristic bright area in figure 2(*a*) clearly indicates the charge build-up; however, no charging effect was observed as shown by the confined dot at the resist surface in figure 2(*b*). Figure 2(*c*)is a schematic diagram of the electron path that leads to secondary electron emission and built-up charges. In comparison, figure 2(*d*) shows the electron path with the existence of a conducting layer. Most trapped and built-up charges are grounded through the layer. Nevertheless, even with the conducting layer, the resolution may still be affected due to electron scattering. In addition to the conducting layer coating, other types of solutions have also been demonstrated, such as the variable pressure EBL [28] (balancing the negative charges by the positive ions created by electron-gas molecule collision) and the critical energy EBL [29] (balancing the injected and ejected electrons). All these methods, described above, bring in either additional sample fabrication steps or extra variable parameters.

Another issue with epitaxial patterning is the incompatibility between the high deposition temperature of epitaxial growth and the low glass-transition temperature of the resist. This problem exists for both photolithography and EBL. To overcome this issue, metallic or ceramic resist materials, with much higher melting points, may be used to replace conventional organic resist. Recently, Banerjee *et al* demonstrated epitaxial patterning of $PbZr_{0.52}Ti_{0.48}O_3$ (PZT) structures on insulating substrates, with AlO_x being the resist material for high temperature processing (figure 3 [30, 31]). Apart from the ability to withstand high temperatures, AlO_x can also be directly patterned with ultra-violet (UV) light, and also subsequently developed by a basic solution that reacts with exposed AlO_x to form water-soluble alkali-metal aluminates. After deposition of desired material, the AlO_x mask is subjected to a liftoff process by using aqueous NaOH solution, in which the AlO_x dissolves as water soluble sodium aluminate. This process is compatible with both photolithography and EBL. Epitaxial patterning using AlO_x masks at the mesoscale (100–1000 nm) has been successfully demonstrated [30, 31]. For EBL epitaxial patterning, the use of AlO_x mask was combined with a Au sandwich layer between AlO_x and PMMA to enhance discharging [31]. However, in principle, other types or combinations of light metal and conducting polymer should also be applicable for this purpose.

These processes demonstrated the key methodology of combining epitaxial growth with lithographic patterning using conventional methods —via the combination of a discharging layer (for insulating substrates) and a ceramic resist (for high temperature deposition). The extension of such processes to the patterning of various other materials is thus expected. It is to be noted that AlO_x is not the only candidate as resist material for high temperature deposition. Some

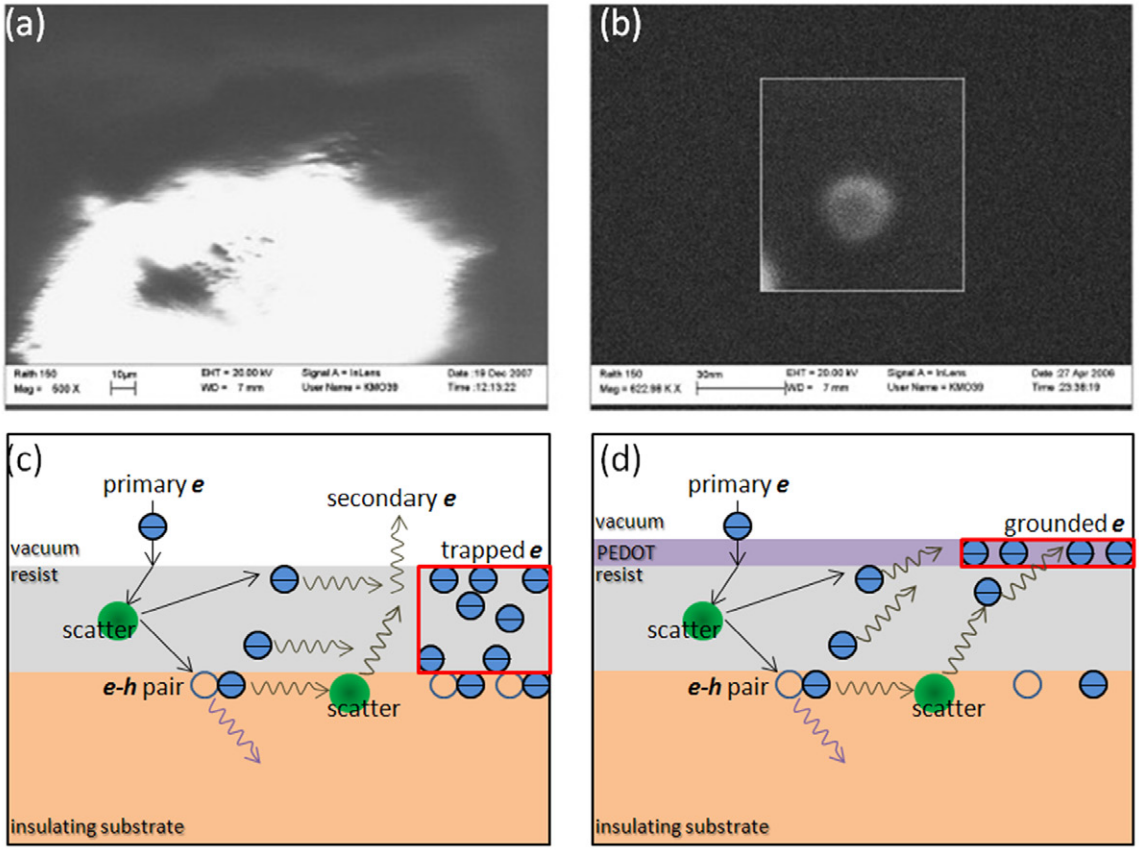

Figure 2. (*a*) SEM image of the quartz substrate sample coated with negative resist after an *e*-beam exposure. It shows a bright surface area caused by the built up surface charge. (*b*) SEM image of the quartz substrate coated with negative resist and PEDOT/PSS. Zoomed window shows an *e*-beam 20 nm dot on the top surface with no surface charging effect. Schematic diagram of electron trajectories (*c*) showing built up charges and (*d*) with PEDOT/PSS top coating showing significantly less built-up charging. Reprinted from [24], copyright (2009), with permission from Elsevier.

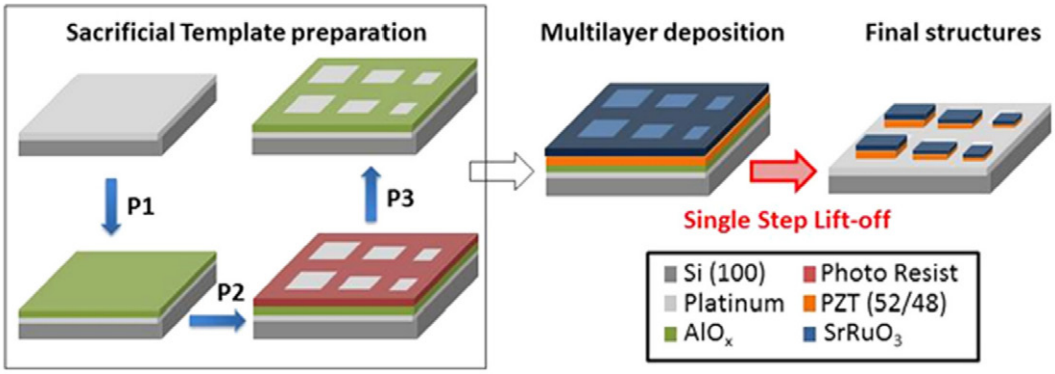

Figure 3. Schematic representation of the patterning process of $PbZr_{0.52}Ti_{0.48}O_3$ film together with epitaxially grown $SrRuO_3$ electrode on platinized Si substrate. Step P1–P3 describes preparation of sacrificial amorphous aluminum oxides (AlO_x) template. Step P1 represents deposition of AlO_x on a platinized Si substrate. Step P2 and P3: photolithographic patterning of template AlO_x layer. Next $PbZr_{0.52}Ti_{0.48}O_3$ and $SrRuO_3$ multilayers were deposited at high temperature by PLD. Finally template layer was lifted-off together with top-grown materials through a base assisted liftoff yielding heterostructured patterns in uncovered areas. Reprinted with permission from [31]. Copyright 2013, AIP Publishing LLC.

metallic 'resist', such as Mo, Cr, and Ti may be favored due to their higher resolution and easier removal, as will be discussed in the following sections. In general, experiments have shown that the epitaxial patterning can be done with photolithography and EBL, but the long-standing issues with photolithography (resolution limited to the photon wavelength) and EBL (low throughput) still limit their application for sub-100 nm and wafer-scale patterning purposes. On the other hand, unconventional lithography methods have experienced significant development in recent years with unique

advantages over photolithography and EBL. These novel techniques also offer new opportunities and perspectives for epitaxial patterning.

2.2. AFM nanolithography

In addition to its well-developed imaging and characterizing capabilities, AFM has also demonstrated good potential for nanolithography. The various capabilities of AFM lithography include modification, deposition, removal, and manipulation of materials for nanofabrication. Depending on the basis of the operating mechanisms, AFM lithography can be classified [32] into two main groups, i.e. force-assisted and bias-assisted nanolithography, where a pure-mechanical-process (force) and an electric-assisted-process (bias) are involved, respectively. Force-assisted lithography relies on direct mechanical process, including indentation, plowing and writing; while bias-assisted lithography encompasses probe anodic oxidation and electrochemical deposition/modification. Owing to the rapid development in AFM hardware, other energy sources in addition to electrical, such as thermal or chemical can also be incorporated on the AFM tip for enhanced fabrication. Interested readers are referred to two review articles for a comprehensive understanding of AFM-based nanofabrication [33, 34].

The electric-bias-assisted AFM lithography has been widely explored due to its simplicity and stability. The manipulation of electric source and components are also relatively straightforward compared to thermal and chemical sources. The experimental setup can be realized by applying a voltage-bias between the AFM tip and the conducting substrate. One of the most extensively-studied mechanisms of bias-assisted lithography is the local anodic oxidation (LAO), where the water meniscus (due to capillary condensation) in the tip-sample gap is dissociated by the negative tip bias, and the O^- and OH^- oxidative ions react with the substrate to form localized oxide nanostructures. LAO has been studied for various materials including semiconductors [35–37], oxides [38–41], metals [42–45], molecular surfaces [46–49], and for the purpose of material deposition, removal, and modification. LAO-induced material removal is probably the most relevant process for general lithography and patterning: the locally-removed material serves as a template for subsequent pattern transfer of desired material. In this sense, LAO of typical lithographic resist, such as PMMA and SU8 have been reported [50–53]. These resist templates can be used for pattern transfer through the general 'deposition-liftoff' process. However, they are usually not thermally robust enough for epitaxial patterning through deposition, which takes place at elevated temperatures. In this sense, certain types of metallic 'resist' are favorable, that are suitable for LAO process and with much higher melting points (T_{melt}), such as Ti (T_{melt} = 1668 °C), Cr (T_{melt} = 1907 °C), and Mo (T_{melt} = 2623 °C). LAO processes on metallic thin films have been reported. For example, Snow *et al* and Held *et al* showed AFM-induced LAO on Ti films and its selective removal for fabrication of quantum point-contact in the nanoscale and mesoscale, respectively [54, 55]; Sugimura *et al* demonstrated nanolithography using LAO on Ti metallic resist. They found that the composition of the anodized pattern is TiO_2, which can be further etched by HF during the final liftoff [56]. Similar studies have been performed also on Cr [57] and Al [58]. However, one of the most promising candidates is Mo, with a much higher melting point than Ti, Cr, and Al. Rolandi *et al* first introduced the LAO of Mo to form MoO_3 patterns that can be subsequently etched by simply using water [59]. The patterned Mo were then used either as an etch mask to pattern underlying material/substrate, or as a resist mask to fabricate nanostructures through deposition and liftoff.

Kawai *et al* extended the application of LAO-induced Mo patterning to the fabrication of epitaxial nanostructures [60–62]. Their process takes advantage of the high melting point of Mo, which allows the deposition (with the Mo template) to be done at elevated temperatures suitable for epitaxial growth. The strong conductivity of Mo also enables decent resolution, ~100 nm, achievable for the AFM lithography. In their experiments, as shown in figure 4, a Mo film was first deposited onto the $Al_2O_3(0001)$ single crystal substrate. MoO_3 lines were then defined using the AFM tip through LAO, which were subsequently removed by immersion in water. The Mo pattern thus obtained was used as a resist for deposition of epitaxial $Fe_{2.5}Mn_{0.5}O_4$ at 340 °C. The Mo mask is stable and therefore retains its shape during deposition. After cooling down to room temperature, the Mo layer was removed in 10 vol% H_2O_2 solution. $Fe_{2.5}Mn_{0.5}O_4$ nanoscale lines were successfully defined in the designated area on the substrate. Goto *et al* further expanded the scope of this technique to the fabrication of single-nanowire devices [63] and nanoconstrained structures [64], in which the magneto-transport measurements are made possible for these epitaxial nanostructures.

The epitaxial patterning using AFM lithography and Mo liftoff can be expanded to a wide range of materials not limited to metals and oxides. The advantages of using AFM lithography include: (1) a mask-free process, sharing the same advantage with EBL; (2) possibility of multi-step lithography by computer programming; (3) positioning of the pattern with greater accuracy without complex alignment steps as in photolithography; (4) performing simultaneous *in-situ* imaging after the lithography without additional sample transfer; (5) ultrahigh resolution (sub-10 nm); and (6) the good LAO performance of Mo makes it very suitable for epitaxial patterning. However, currently the biggest limitation for this technique is its low speed and low throughput, which make it unfavorable for industrial mass production. This issue may be solved by operating multiple tips in parallel, or by increasing the tip writing or scan speed. Future work should emphasize this aspect of the technique.

2.3. Nanostencil lithography

Nanostencil lithography (NSL) describes the direct deposition, etching, or ion implantation of materials through a pre-patterned mask—often called a stencil—to achieve the patterning of desired materials. Stencils are just shadow-masks in a general sense; however, modern stencils have evolved such that they are suitable for many different applications. It has been widely

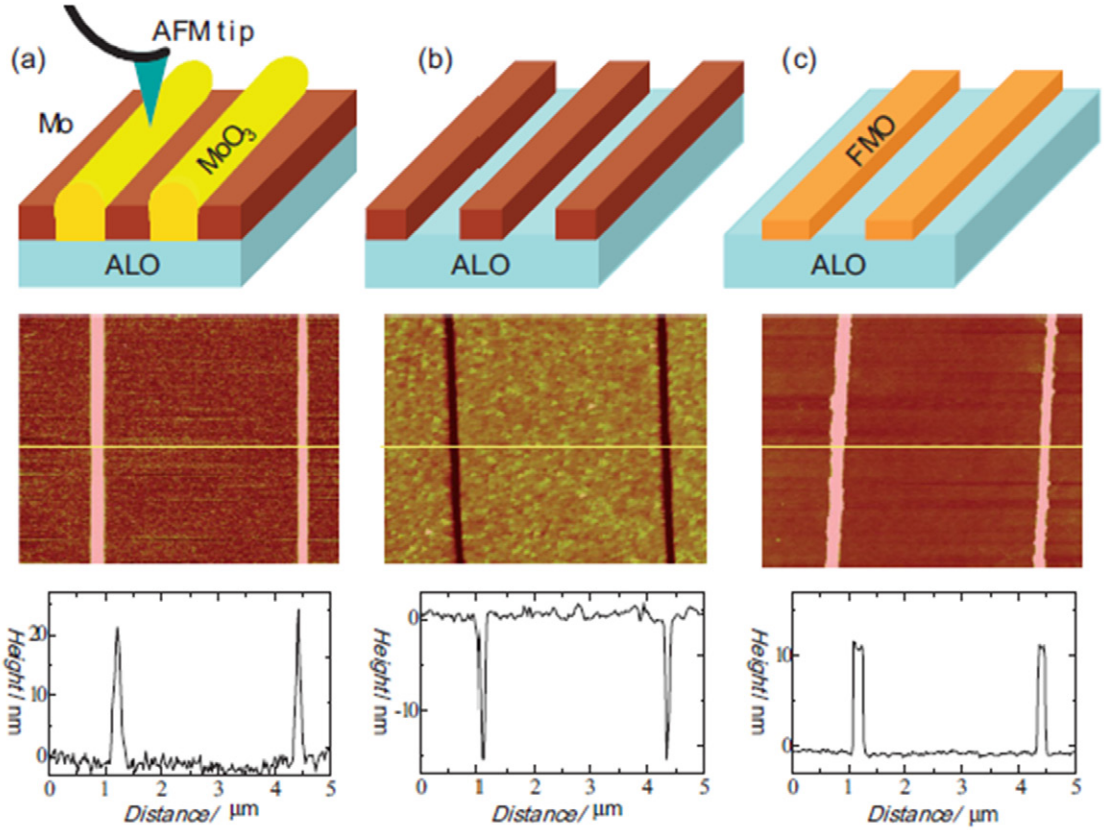

Figure 4. Mo liftoff process used for the fabrication of oxide nanostructures. The top panel schematically illustrates the steps involved in the process. The middle panel shows topographic images of line patterns fabricated by this process. The bottom panels depict the cross sections of the line patterns shown in the middle panels along the yellow lines. Reproduced with permission from [61]. Copyright 2008 Wiley-VCH Verlag GmbH & Co KGaA.

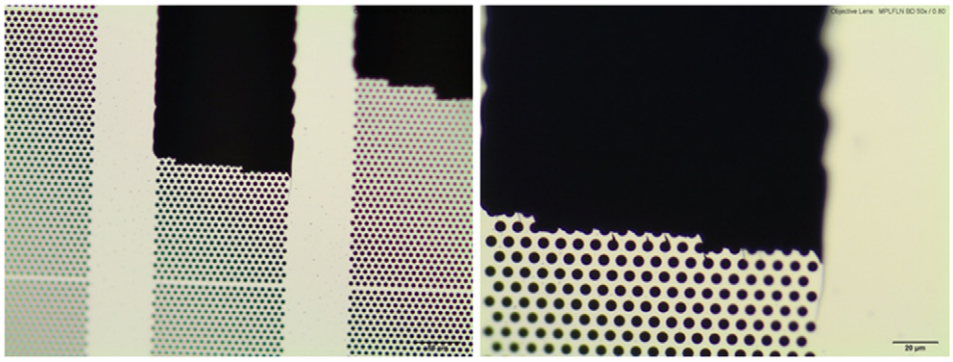

Figure 5. Photograph image of a commercial Si_3N_4 nanostencil membrane (featuring 5 μm circular aperture arrays) from Aquamarijn Micro Filtration BV.

used in microelectronics, bio-technology, and nanotechnology, and can allow fabrication of structures at sub-100 nm resolution. The most attractive feature of NSL is perhaps the fact that it is a resist-free lithography. On one hand, since the material is deposited directly onto the substrate, any pre-treatment for the substrate and heat load and/or chemical interactions arising from resist processing are absent; this allows simple fabrication of high-quality structures that are atomically clean. On the other hand, the deposition condition can be kept the same as that for continuous thin films, which ensures a minimal deviation of the chemical structures and properties from the thin-film samples. These features make NSL quite favorable for epitaxial patterning. Recently, different operating modes for NSL have been also demonstrated: apart from the conventional static mode where the stencil is aligned and fixed onto substrate, the multistep and dynamic modes enable nanostencils to move relative to the substrate in between and during depositions, respectively [65–72]. These additional modes also bring new capabilities for NSL that include: (1) fabrication of multi-mask and multi-material structures; (2) fabrication of arbitrary 2D geometries; (3) varied material thicknesses and/or structures using the same stencil.

A number of different materials can be used for nanostencils, including metal, Si, Si_xN_y, and polymer. The most widely used material is probably Si_3N_4 membranes [73]; there are also increasing reports of NSL using inexpensive, easy to fabricate anodic aluminum oxide (AAO) nanostencils [74–77]. Nanostencil apertures can be defined by laser interference lithography [78], electron beam lithography [79], focused ion beam lithography [80], and local anodic oxidation [81, 82]. Nanostencils are usually made very thin, with a thickness around hundreds of micrometers. They are also very fragile and need to be handled carefully. Figure 5 shows an example of a commercial Si_3N_4 nanostencil membrane featuring 5 μm circular aperture arrays.

Since nanostencil fabrication is a non-trivial process, the reusability of a nanostencil is quite important to make this technique truly cost-effective. However, one intrinsic issue that affects the lifetime of a stencil is the clogging effect: during deposition through the stencil, material is deposited not only on the substrate through the apertures, but also on the backside of the stencil, including around and inside the apertures. This effect gradually reduces the effective aperture size of the stencil and leads ultimately to aperture clogging. For example, Takano *et al* showed that about 50% of the intended thickness of the deposited metals was deposited on the sidewalls of the apertures [83]. The clogged stencil apertures are clearly illustrated in figure 6. In addition, heavily deposited metal also induces mechanical stress to the stencil and further causes the membrane to deform around the aperture edges. These effects related to clogging are probably acceptable for patterning microstructures and for low-throughput fabrication (Laboratory R&D); however, in order to apply this technique to large-scale industrial production, cleaning treatments to recycle clogged stencils are necessary. Significant effort has been put to increase the lifetime of nanostencils. This can be done by either the selective removal of deposited material from the stencil, or the functional coating on the stencil prior to deposition. For example, Vazquez-Mena *et al* demonstrated *ex-situ* cleaning of nanostencils using wet-etching. In the case of Al deposition through a Si_3N_4 membrane, the clogged aperture can be cleaned in a solution of CH_3COOH (100%), HNO_3(70%) and H_3PO_4(85%) in proportions 5:3:75, which has a good etching selectivity of Al to silicon nitride [84]. Yan *et al* demonstrated functionalized coating for reduced clogging from Pt deposition. Specifically, the stencil surface is functionalized by tridecafluoro-1,1,2,2-tetrahydrooctyl-1-trichlorosilane (FTS) prior to use to form a fluorine-terminated self-assembled monolayer. The low-surface-energy FTS helps to reduce the incident Pt metal from sticking to the stencil. It also serves as a protective layer during stencil cleaning after the stencil has been used for a few Pt depositions [85].

Another challenge with NSL is known as 'blurring', i.e. the unfaithful pattern transfer (usually an enlargement of the initial pattern) from the stencil to the substrate. This could come from the geometry of deposition, including the directionality of deposition flux and the physical gap between the stencil and substrate [86]. The influence of the stencil-substrate gap on the blurring effect is clearly illustrated in the nice

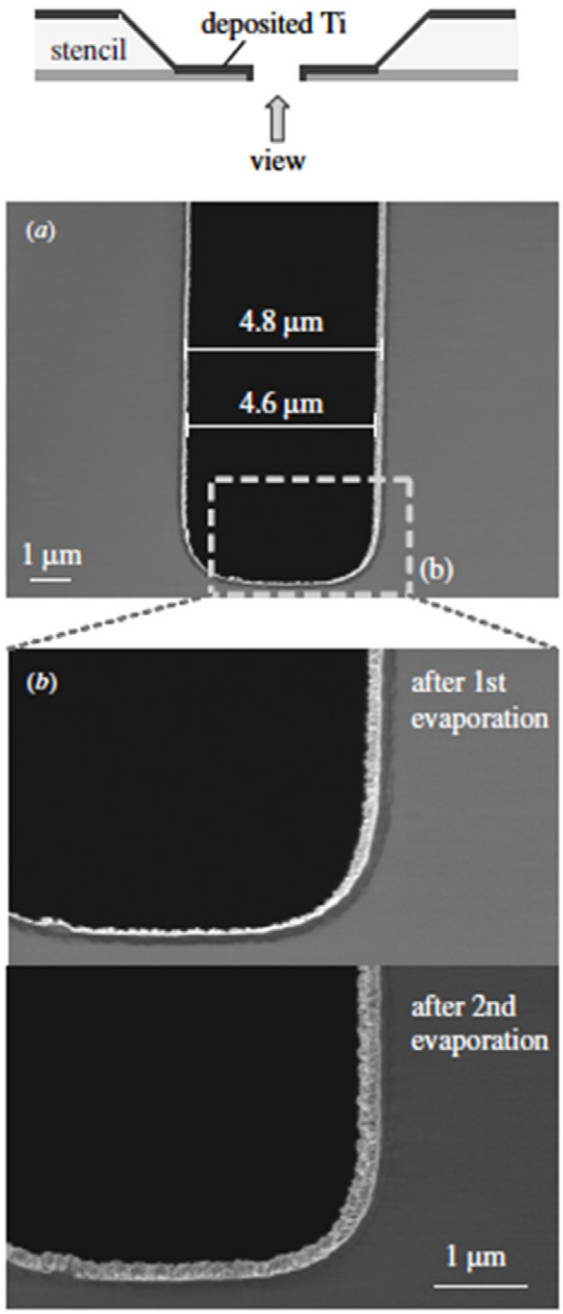

Figure 6. SEM images of the microstencil observed from the side having faced the substrate during the evaporation; (*a*) after first evaporation, (*b*) enlargement of a part of (*a*) indicated by the dotted rectangle, after first and second evaporations (200 nm/evaporation) of Ti. Progress of the clogging at the edge of aperture can be clearly observed. Reprinted with permission from [83]. Copyright 2006 Institute of Physics Publishing.

experiment done by Takano *et al* [83], where a SU-8 layer is used to tune the gap between a Si substrate and a microstencil. The deposited structures with and without the gap is compared in figure 7. A quantitative, geometrical analysis for the blurring effect can also be found in [83]. Figure 8(*a*) is a simple schematic illustration of the blurring effect of deposited structures when a gap is present between a stencil and a substrate. The evaporated metal flux from a typical point source is modeled as a straight line from the source to the substrate,

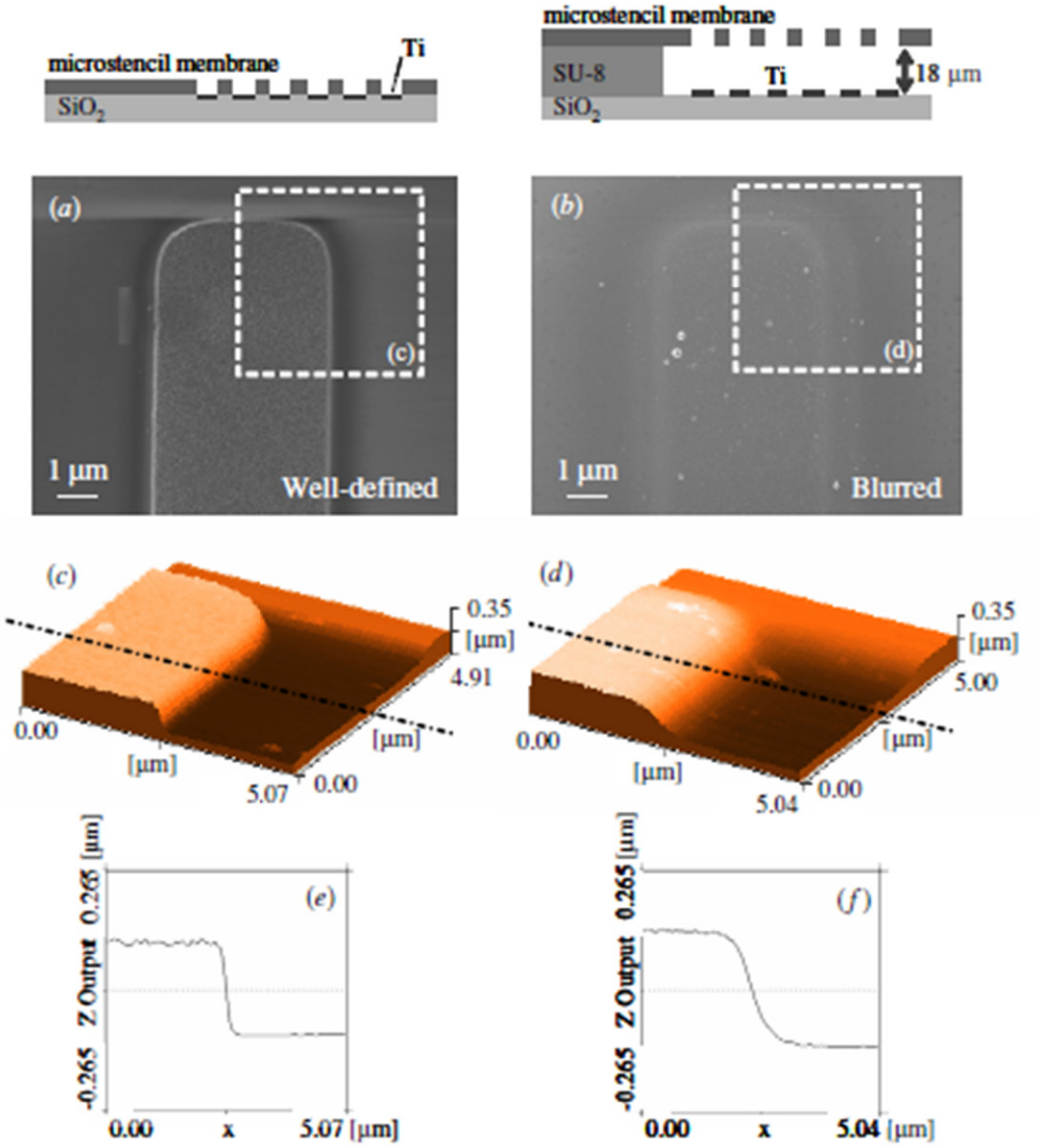

Figure 7. Comparison of Ti microstructures deposited on the same material surface (SiO_2) without and with a gap: SEM images, shown with schematic cross-sectional illustration of the sample setup during the evaporation, (*a*) without SU-8 spacer and (*b*) with 18 μm thick SU-8 spacer. (*c*) and (*d*) AFM images of a part of figures (*a*) and (*b*) (indicated by dotted square), respectively, (*e*) and (*f*) cross-sectional line views of the AFM images in (*c*) and (*d*), indicated with broken lines. Reprinted with permission from [83]. Copyright 2006 Institute of Physics Publishing.

since the mean free path of evaporated metal particles is usually much longer than the distance between the source and the substrate. Depending on the deposition geometry, evolution of the blurring effect can be quite significant over the lateral dimension of the substrate. Gradually enhanced blurring effect can be even observed over several micrometers as shown in figure 8(*b*). Last but not least, the blurring effect can be also due to the surface diffusion of the arriving species on the non-restricted substrate surface [87]. This effect becomes more significant during epitaxial patterning since the substrate temperature is usually quite high, giving higher mobility to the arriving adatoms. The high temperature may also induce thermal stress to the stencil, resulting in the membrane deformation similar to the situation with the mechanical stress, such as membrane stretching and shrinking. To reduce the blurring effect, the most effective approach is to minimize the gap between the substrate and the stencil. This can be done by engineering special substrate-stencil holder [88] with precise position control of the stencil relative to the substrate. Such holders also help to avoid tilting of the stencil with respect to the substrate surface to ensure a constant gap distance across the whole substrate. Alternatively, one could also develop the stencil mask directly from the substrate by chemical synthesis [74]; however, such stencil may only be used once and can be subsequently disposed by selective etching (lift-off). In addition to the gap control, increasing the distance between substrate and source, as well as reducing the thickness of the stencil membrane also helps to mitigate the blurring effect. Figure 9 provides a visual summary of all the parameters that determine a faithful pattern replication using NSL.

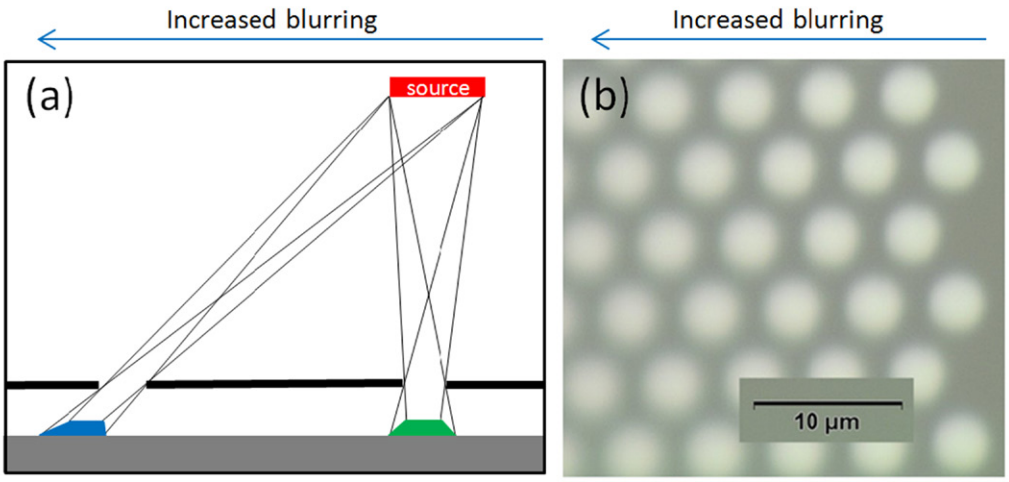

Figure 8. Schematic illustration of the blurring effect of deposited structures when a gap is present between a stencil and a substrate. (*b*) Photograph image of deposited metal structures through a stencil featuring 3 μm circular aperture arrays. The substrate-stencil gap is 0.5 mm, and the distance between substrate and source is ~40 cm.

Since NSL requires neither resist coating nor substrate-pretreatment, it can be applied directly for high-temperature, epitaxial patterning on single-crystal and/or functionalized substrates. High temperature, epitaxial patterning using NSL was demonstrated by Shin *et al*, where epitaxial $Pb(Zr_{0.2},Ti_{0.8})O_3$ was deposited on a $SrRuO_3$ film on a $SrTiO_3(001)$ substrate, at 760 ºC through a Si_3N_4 stencil mask [89]. The Si_3N_4 membrane was used as a stencil because it can withstand temperatures as high as ~800 ºC. The nano-pore arrays (~100 nm dia.) on the Si_3N_4 mask was defined by e-beam lithography and RIE process. Epitaxial $Pb(Zr_{0.2},Ti_{0.8})O_3$ nanodot arrays were successfully demonstrated; however, the parameters influencing the lithography process were not discussed in detail. Cojocaru *et al* investigated NSL patterning combined with PLD of various materials including metals (Pt, Cr), semiconductors (Ge), and complex oxides ($BaTiO_3$ [90–92]), in which the desired materials are directly deposited through the stencil mask on the substrate. In order to avoid the substrate-stencil gap, Morelli *et al* deposited an array of Al dots through a stencil on a $BiFeO_3$ film and used the Al dot array as an etch mask for epitaxial patterning $BiFeO_3$ nanostructures through FIB [93]. Such etch masks can also be defined by stencils obtained from self-assembly, such as monolayer of ordered microspheres [94] or nanoparticles [95].

Nechache *et al* showed controlled epitaxial patterning of Bi_2FeCrO_6 nanostructure arrays on Nb-STO(100) substrate using PLD at a substrate temperature ~650 ºC [96, 97] (figure 10). The nanostencil used in the experiment, featuring 400 nm circular apertures in a hexagonal array, was defined by laser interference lithography. An intimate contact between the stencil and substrate was achieved by using a proper mechanical fixture. Thus, the blurring effect due to deposition geometry is minimized. Nevertheless, a broadening of structure sizes was still observed and was attributed to both geometrical broadening and, more importantly, to the lateral surface diffusion of species impinging with relatively high kinetic energies at high temperature (figure 9(*c*)). The existence of the surface diffusion of species was confirmed by the equilibrium-shapes of the resulting Bi_2FeCrO_6 nanodots. Specifically, the nanodots all display a *rectangular* shape even with *circular* apertures of the nanostencil. This is because the kinetic energy and the surface mobility of the absorbed species are high enough to induce nucleation and crystallization for the epitaxial nanodots to favor their lowest surface energies on the {100} facets. As a result, for epitaxial patterning using nanostencil lithography, the shape of the structures may be determined primarily by their crystalline preferences instead of the nanostencil aperture. This may lead to certain limitations if one wants to study a specific shape and at small scales. Nevertheless, NSL is one of the most promising techniques for epitaxial patterning due to its resist-free implementation, simplicity, and cleanliness, plus its uncomplicated deposition of various other metals, oxides [98], and multi-layer structures [99].

2.4. Nanoimprint lithography

Nanoimprint lithography (NIL) is an unconventional lithography technique for high-throughput, high-speed patterning of polymer nanostructures with great precision and low cost [100, 101]. NIL relies on direct mechanical deformation of the resist material under a 'rigid' stamp and therefore avoids expensive electron or photon sources required in EBL or photolithography, respectively. In addition, it can achieve resolutions beyond the limitations set by light diffraction or beam scattering that are encountered in the conventional techniques. NIL has experienced numerous developments in the past decade due to its wide range of applications in electronics, photonics, data storage, and biotechnology. Interested readers are referred to the following reviews for the recent developments of NIL in various research fields [102–107].

Unlike EBL and photolithography, NIL uses a mechanical approach to generate resist patterns with the advantage of using a process independent of the substrate electrical conductivity. Therefore, NIL is compatible with process on many unconventional substrates, including insulating substrates that are usually encountered in epitaxial growth. In

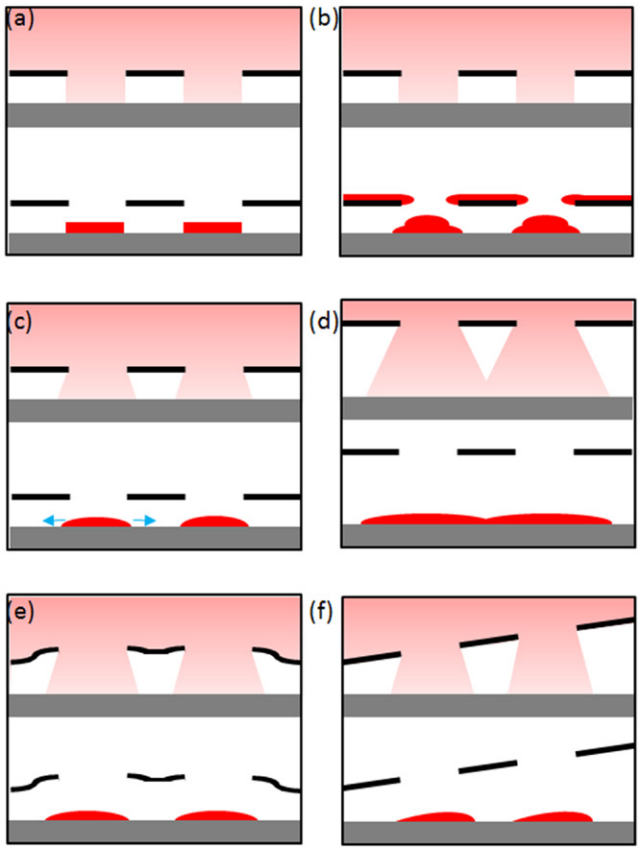

Figure 9. Schematic illustration of the parameters influencing the faithfulness of the pattern transfer using NSL. (*a*) ideal situation; (*b*) clogging effect may reduce the size of the aperture and the resulting material structures; (*c*) imperfect deposition directionality and surface diffusion may cause blurring effect; (*d*) such an effect can become more severe as the stencil-substrate gap increases; (*e*) mechanical and/or thermal stress may cause the stencil to deform and affect the deposited structures; (*f*) tilted stencil (relative to the substrate) may cause structure inhomogeneity and large-area non-uniformity across the substrate.

order to withstand the high temperatures during deposition, metallic resist with high melting point, such as Mo, is recommended. An appropriate metallic negative-mask (e.g. ordered hole array) can be achieved by direct deposition through a resist mask with an opposite tone (e.g. ordered pillar array). For example, Suzuki *et al* reported a pioneering NIL-based epitaxial patterning of $Fe_{2.5}Mn_{0.5}O_4$ nanodot arrays, using a metallic Mo mask that was created via depositing Mo onto a pre-fabricated polymer mask [108]. The polymer mask was generated by typical UV-NIL process and etching. The process is illustrated in figure 11. The $Fe_{2.5}Mn_{0.5}O_4$ deposition is conducted at 340 °C to result in an epitaxial film. The Mo liftoff was achieved using 10–30 vol% H_2O_2 solution under a brief ultrasonication. The chemical etching mechanism based on general reactions between amorphous Mo and H_2O_2 is:

$$\mathrm{Mo(amorphous)} + \mathrm{H_2O_2} \rightarrow \mathrm{MoO_4^{2-}} + 2\mathrm{H^+} + \mathrm{H_2\,(gas)}.$$

This reaction usually yields very clean liftoff for the final epitaxial nanostructures. The method was quickly extended to epitaxial patterning of other oxides [109, 110] and metallic structures [111]. Such process demonstrated a basic protocol for epitaxial patterning using NIL. However, the imprinting yield of the stamp and the properties of the Mo mask were not discussed in detail, which are important aspects for large-area, high quality epitaxial patterning. We address these two factors in the following sections.

2.4.1. Soft stamps for defect-free epitaxial patterning. In this section, we focus on improving the imprint yield for epitaxial patterning using soft working stamps. The properties of epitaxially patterned structures are much more easily influenced by extrinsic parameters, such as defects generated from the lithography process. For example, submicron-size particles in the resist solution that are not filtered-out can be transferred onto the substrate after spin coating, causing local failure of lithography and defects in the pattern. In epitaxial magnetic nanostructures, these defects can act as extrinsic nucleation centers for magnetic domain walls. Actually, the consequence of such defects can be quite significant for resist-based lithography, especially for NIL that uses direct mechanical contact between a stamp and the resist for pattern generation. In this case, particle-like defects may not only fail to produce a high fidelity reproduction in the resist pattern but also cause serious damage to the precious stamp. Furthermore, it also raises a dilemma for NIL: on one hand, a stamp should be used as many times as possible provided it preserves patterning quality; on the other hand, stamps should not be considered as consumables because of their high cost. One solution to this dilemma is to make high fidelity copies of the stamp from inexpensive materials and use these copies, also known as 'working stamps', for direct NIL practice on resist-coated wafers. In this sense, soft, flexible stamps made from inexpensive polymer-based materials have proven to be quite promising for large-area, defect-free NIL. Typical materials include polydimethylsiloxane (PDMS), Perfluoropolyether (PFPE), Ethylene(tetrafluoroethylene) (ETFE), polyethylene terephthalate (PET), and inorganic–organic hybrid polymers (e.g. Ormostamp®). In addition to their low cost, these soft, flexible stamps offer intimate, conformal contact between substrate and stamp without the need for high external pressure. Their flexibility also makes them insensitive to particle contaminants in the resist, as they can locally deform around a particle without damaging the stamp itself or affecting the lithography yield [106]. Two typical soft stamps that have been studied in epitaxial NIL research are introduced in this review. However, it should be noted that the discussions here can be also expanded to many other types of polymer stamp materials.

2.4.2. Ethylene tetrafluoroethylene (ETFE). ETFE belongs to the family of fluorinated polymer materials. In general, fluorinated polymers have a number of outstanding advantages for soft stamps including very low surface energy, suitable Young's modulus, good mechanical strength, and good chemical stability. Fluorinated polymers were first used to replace PDMS-based polymers for cleaner and finer soft- and imprint-lithography [112, 113]. However, these stamps were used for low pressure and room temperature NIL process, and may not be suitable for thermal-NIL resist and/or inorganic resist.

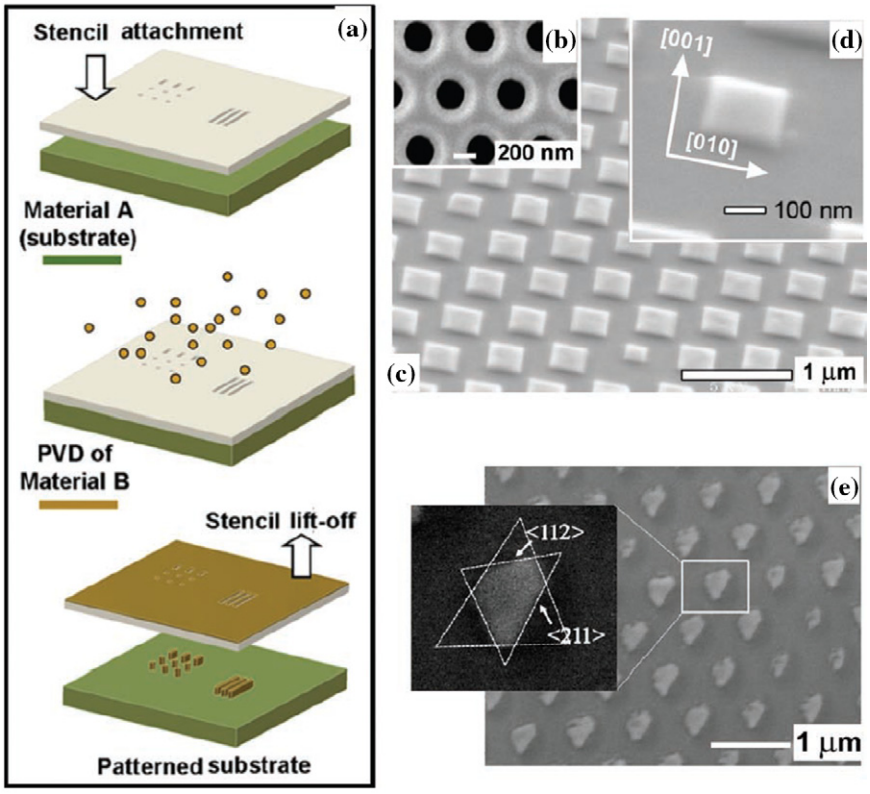

Figure 10. (*a*) Schematic of the nanostenciling process (PVD stands for physical vapor deposition). (*b*) SEM image of a typical Si_3N_4 membrane nanostencil. (*c*) SEM image showing a well-defined array of square Bi_2FeCrO_6 nanostructures approximately 400 nm in lateral size that perfectly retained the hexagonal pattern of the shadow mask. (*d*) Detail of an island of about 150 nm in lateral size, formed because of premature clogging of some apertures. (*e*) SEM micrograph displaying a well-defined array of (111)-oriented Bi_2FeCrO_6 nanostructures. Reprinted with permission from [96]. Copyright 2011 Wiley-VCH Verlag GmbH & Co KGaA.

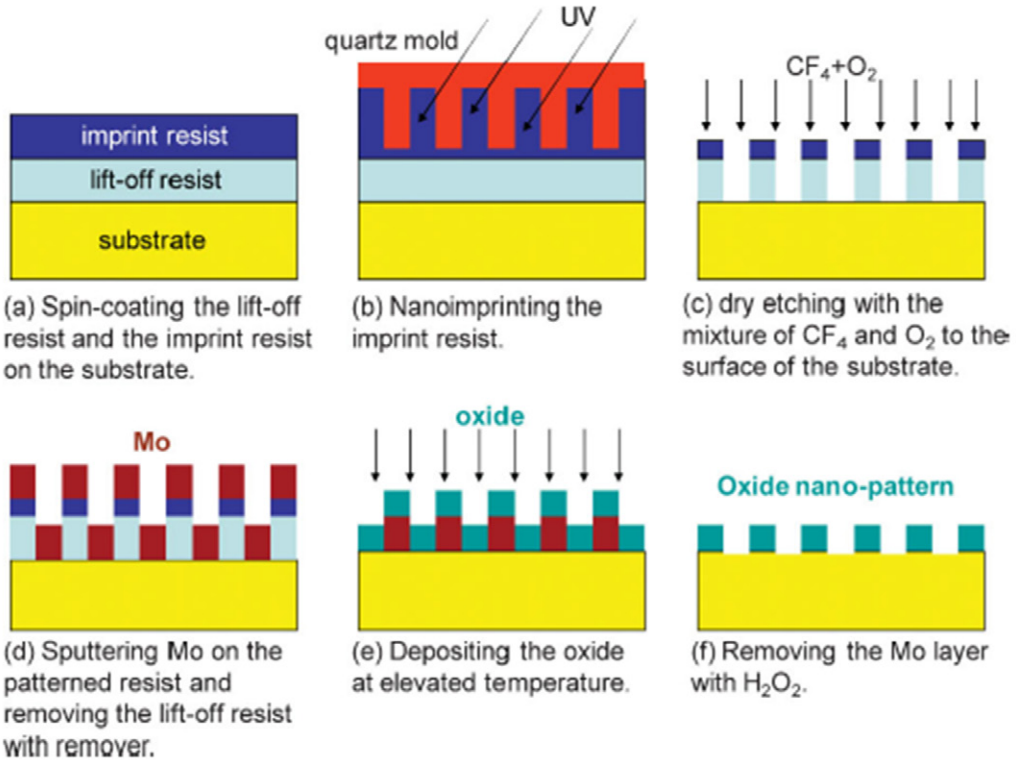

Figure 11. Entire flow process of the NIL-based Mo liftoff technique. Reprinted with permission from [108]. Copyright 2008 Wiley-VCH Verlag GmbH & Co KGaA.

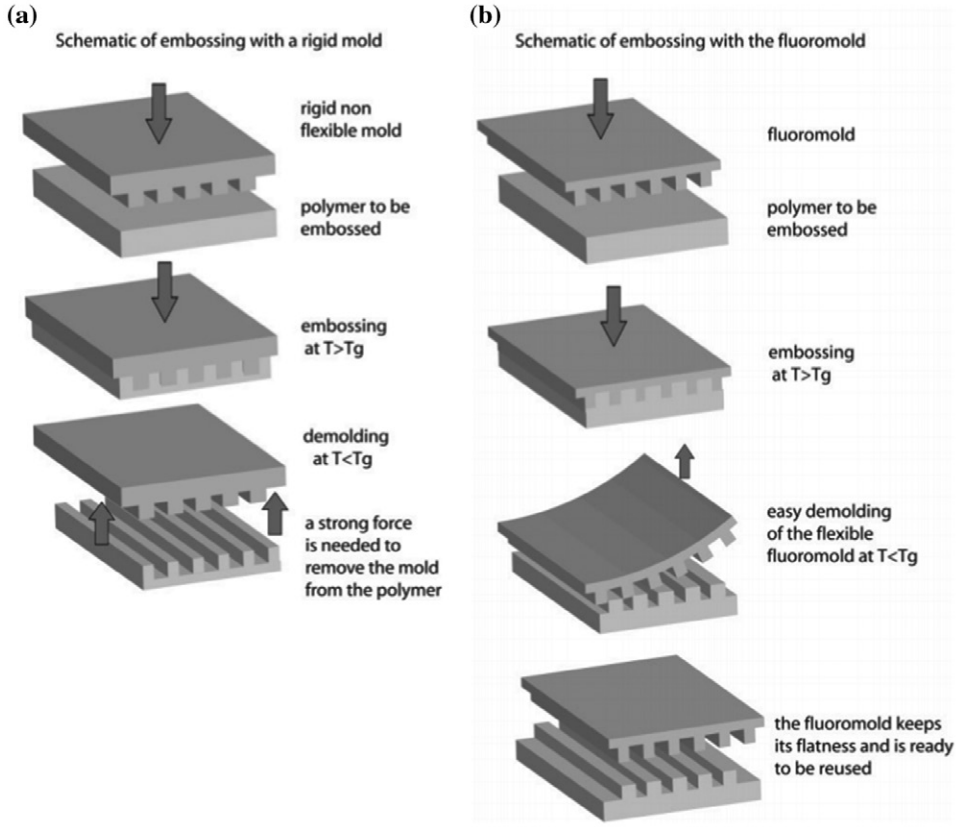

Figure 12. (*a*) Schematic diagram of embossing using a rigid stamp (mold). The polymer and the structured rigid mold are heated above T_g while a pressure is applied to ensure flow of the polymer and to fill the cavities of the mold. Upon cooling below T_g, the entire surface of the mold in contact with the polymer must be separated at once. The relatively strong force required often leads to breaking of the stiff mold. (*b*) Schematic diagram of embossing with a flexible fluoro-mold. During cooling and demolding, the fluoro-mold is bent and gradually separated from the substrate using only a small force since it doesn't adhere to the polymer. The fluoro-mold does not break or deform, and can therefore be reused several times. Reprinted with permission from [114]. Copyright 2008 Wiley-VCH Verlag GmbH & Co KGaA.

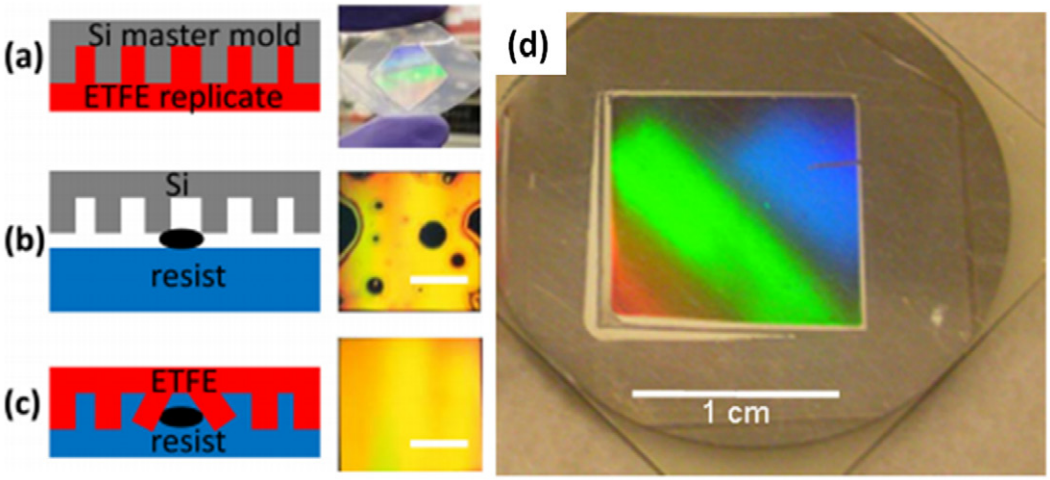

Figure 13. (*a*) Flexible ETFE replica fabricated by a Si master mold; (*b*) wafer imprint with a Si mold; (*c*) wafer imprint with ETFE mold (scale bar: 5 mm). Reprinted with permission. [116] Copyright 2012 American Institute of Physics. (*d*) Photograph of large area imprinted polymer wire arrays (after Mo deposition). Reprinted with permission from [111]. Copyright 2011 Institute of Physics Publishing.

To solve this issue, Barbero *et al* demonstrated ETFE stamps for high-temperature thermal NIL [114]. ETFE is a copolymer of ethylene and tetrafluoroethylene. It has an exceptional toughness and flexibility, high thermal stability, and superior mechanical properties compared to Teflon. Since ETFE has a high melting point in the range of 255–280 °C, it can be readily applied for imprinting most thermal NIL resist, such as Nanonex series (Nanonex Corporation), mr-I series (Microresist Technology), Poly(methyl methacrylate) (PMMA), polystyrene (PS), and inorganic resist such as hydrogen

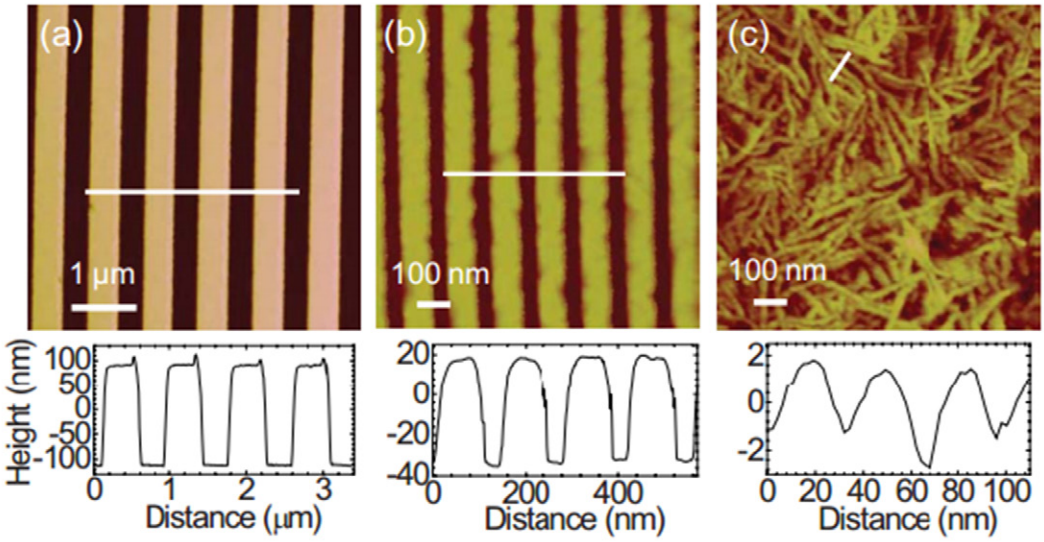

Figure 14. AFM topography images and profiles (along white lines) of ETFE molds with (*a*) 833 nm period, (*b*) 139 nm period, and (*c*) nominally flat mold showing needlelike crystals. Reprinted with permission from [115]. Copyright 2010 American Vacuum Society.

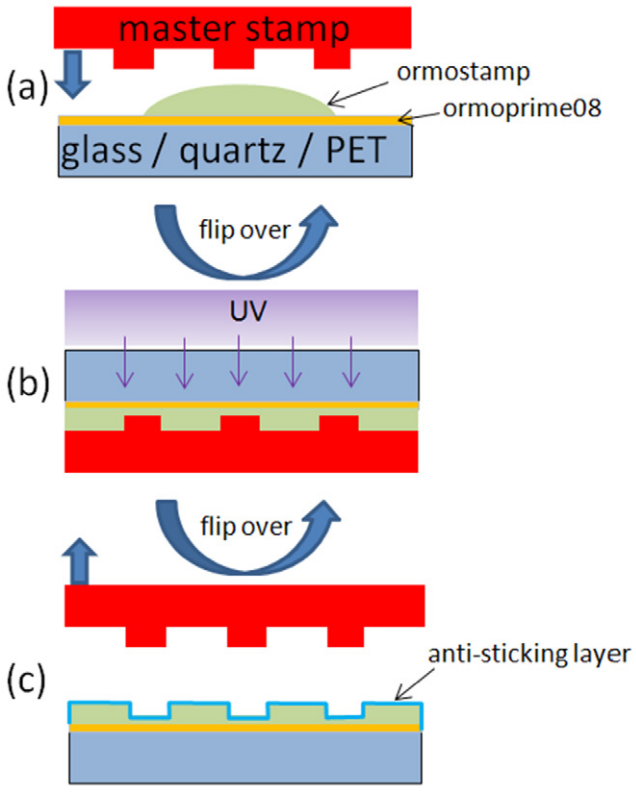

Figure 15. Illustration of the Ormostamp (working stamp) fabrication process. (*a*) stamp preparation: ormoprime08 is spin coated on the substrate followed by the application of Ormostamp on top; (*b*) stamp curing: the sample stack is flipped over and cured under UV light; (*c*) stamp separation: the master stamp is carefully separated with the Ormostamp. Application of anti-sticking layer on the Ormostamp is required before use.

silsesquioxane (HSQ) or TiO_2. In addition, the low surface energy adds benefit of low-adhesion and easy-demolding. The anti-sticking layer that is required for many stamp materials is unnecessary for ETFE. Figure 12 compares the NIL processes using a conventional rigid stamp and an ETFE working stamp. The ETFE working stamps can be made by hot embossing ETFE sheets with a rigid master stamp such as a Si master mold, at a temperature close to the melting point of ETFE. For example, Weiss *et al* demonstrated ETFE replication of a Si master stamp at a temperature ~250 °C and a pressure ~450 psi using a commercial nanoimprinter [115].

We first applied the ETFE stamp for epitaxial patterning with NIL [111]. The semi-transparency and flexibility of as-fabricated ETFE working stamp is illustrated by the photograph in figure 13(*a*). The imprinting results using conventional-Si and soft-ETFE stamps are compared in figures 13(*b*) and (*c*). Direct application of Si stamp on the resist yields significant defect generation, as shown in figure 13(*b*) [116]. Even tiny defects between the mold and wafer lead to visibly large unimprintable areas, due to the rigidness of both the wafer and the stamp. Unpredictable but significant defects in the form of pinholes and thin strips were observed. These defects can be transferred to the final deposition and liftoff, resulting in unwanted thin-film objects (large particles, irregular film pieces, etc). In addition, the issue with defects gets more significant as the stamp is used again and again. This disadvantage casts substantial limitation on potential process scaling. On the other hand, by using ETFE working stamp, the local defects can be accommodated due to the flexibility of the stamp. After imprinting, the demolding is also much easier for the ETFE due to its low surface energy. Defect-free imprints were achieved nearly on the entire stamping area (>1 cm^2) (figure 13(*c*)), which is ideal for epitaxial patterning purposes. High quality imprints on single-crystal MgO substrate (after metallization) is demonstrated in figure 13(*d*) [111].

ETFE working stamps have been experimentally proven to be efficient for mesoscale and microscale patterning (figure 14(*a*)). However, at the sub-100 nm scale the intrinsic ETFE crystallization may prevent a faithful replication of the ETFE from the original master stamp and this should be taken into

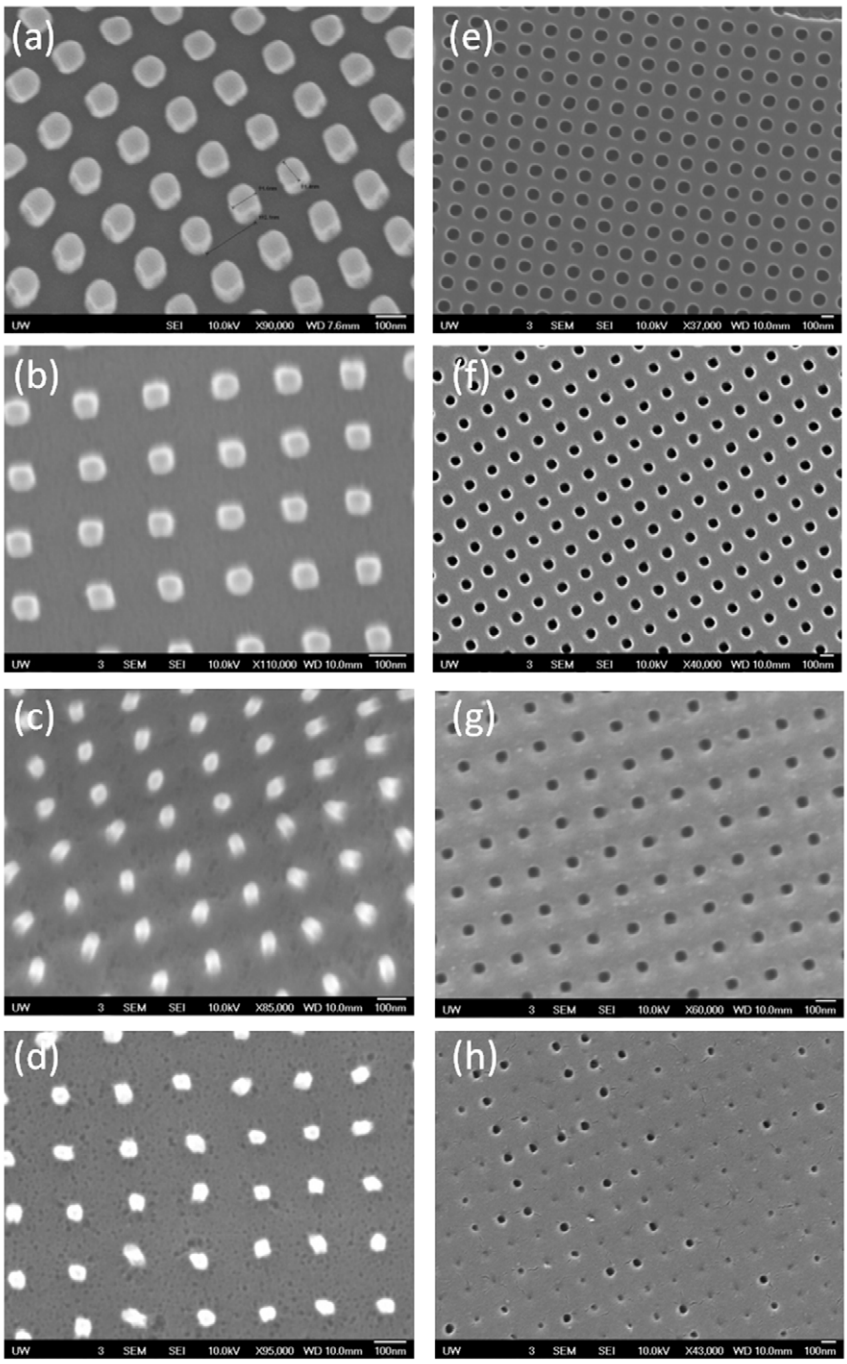

Figure 16. Ormostamp® replications copied from a quartz master stamp featuring 100 nm square dot array, and subjected to oxygen plasma RIE for 1 min at different rf powers: (*a*) no-etch, (*b*) 25 W, (*c*) 50 W, and (*f*) 75 W. Their corresponding imprints on mr-I 7010R resist (Microresist Technology) are illustrated in (*e*), (*f*), (*g*), and (*h*). Note that the magnification is x95000 and x43000 for left and right columns respectively.

consideration. Weiss *et al* revealed a thermal-driven ETFE crystallization by inspecting AFM topographies of ETFE stamps that were fabricated using different Si masters [115]. They found that the ETFE sheet embossed with a flat Si wafer exhibits rod-shaped crystalline domains spaced 20–40 nm apart, with a height between 2.5 nm and 5 nm (figure 14(*c*)). These needle-like grains are also likely accountable for the sidewall roughness of the ETFE features observed in figure 14(*b*). Such crystallization of ETFE under hot-embossing conditions limits the spatial resolution and therefore the performance of ETFE working stamps. To work with sub-100 nm features, one may have to turn to other types of polymers such as Ormostamp as proper working stamp materials.

2.4.3. Ormostamp®. Ormostamp® (Microresist Technology) is a promising working stamp material for sub-100 nm epitaxial patterning. Ormostamp is made of UV-curable inorganic-organic hybrid polymers, and its UV transparency and thermal stability makes it suitable for both UV and thermal

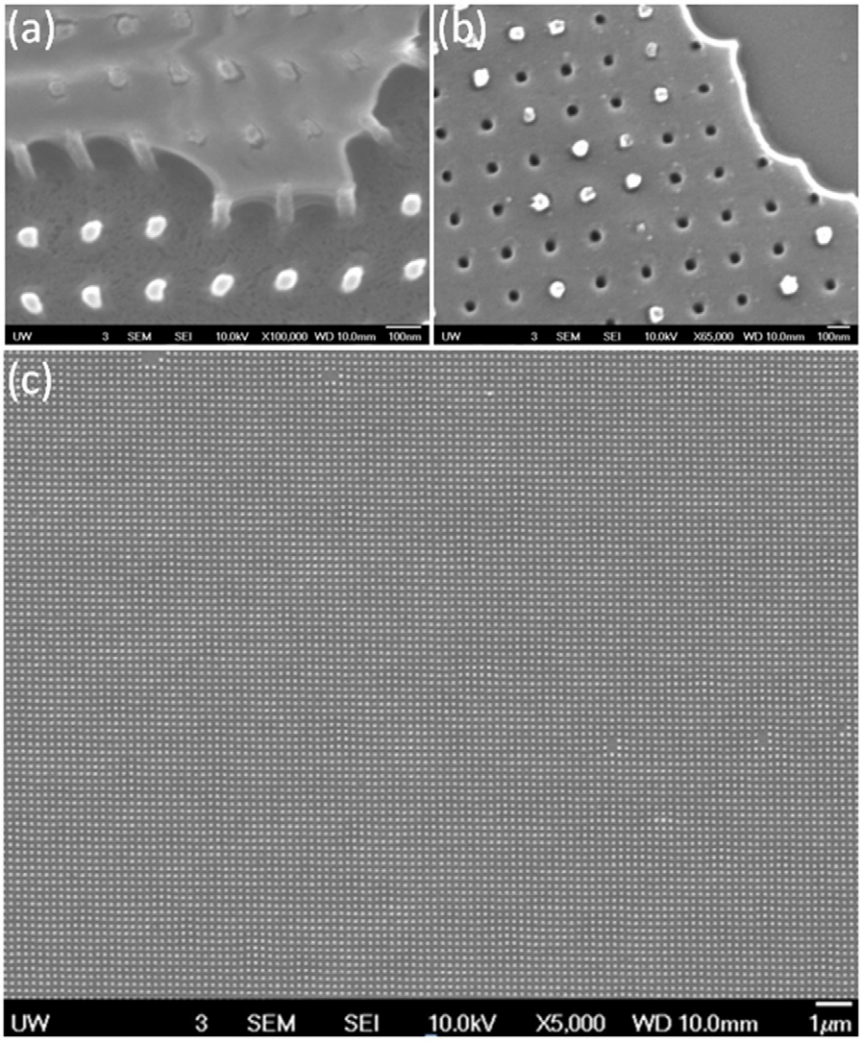

Figure 17. Effects due to low-adhesion issues after demolding. (*a*) Resist peels off and sticks to the Ormostamp features. (*b*) Ormostamp pillars detach from the holding stamp and stick to the resist. (*c*) Large-area sub-100 nm nanodot arrays obtained from a high quality demolding process.

NIL practices. Ormostamp is gel-like before curing, with relatively low viscosity that enables efficient filling of the master template cavities. After UV curing, it acquires sufficient hardness and good elasticity, which allows for patterning high quality, sub-100 nm structures without inducing cracks and fractures. In addition, unlike ETFE, a cured Ormostamp can be used as a master stamp for making new working stamps; therefore the tone of the stamp can be changed from positive to negative and vice versa. The fabrication process of the Ormostamp is shown in figure 15. The gel-like Ormostamp is cast either on the master stamp or a clean substrate (glass, quartz, or PET) pre-coated with Ormoprime08 (Microresist Technology)—an adhesion promoter for Ormostamp (figure 15(*a*)). The Ormoprime08 can be applied by conventional spin coating. The 'master stamp-Ormostamp-substrate' stack is then UV cured and thermally annealed (figure 15(*b*)). To perform NIL with Ormostamp, the anti-sticking layer, trichloro(1H,1H,2H,2H-perfluorooctyl)silane, is subsequently applied by vacuum evaporation (figure 15(*c*)). Excellent pattern transfer fidelity has been demonstrated for sub-100 nm structures [117–119].

We studied a number of properties of Ormostamp in the context of patterning epitaxial films. For defect-free process, transparent and flexible plastics such as PET, rather than glass or quartz, are preferred as host substrates for the Ormostamp features. We demonstrated Ormostamp copies on PET substrate and their corresponding imprints, as shown in figure 16. An advantage of Ormostamp is that the feature size can be controllably reduced by oxygen plasma etching. For example, we replicated an Ormostamp from a quartz master stamp featuring 100 nm square dot array. After UV and thermal curing, the Ormostamp were cut into four pieces and subjected to O_2 plasma RIE for 1 min, at 1 Torr, and at different rf powers (no-etch, 25 W, 50 W, and 75 W), as shown in figures 16(*a*)–(*d*). Figures 16(*e*)–(*h*) show the corresponding imprints using the above working stamps. We found that the feature size of working stamps and therefore the corresponding imprints gradually reduces as the rf power increases. As a result, the RIE process allows tunable feature size of the Ormostamp made from a single master stamp, and can therefore even reduce the cost of the master stamp fabrication. Nevertheless, a reliable aspect-ratio of the Ormostamp features needs to be maintained during the RIE. In our case, if

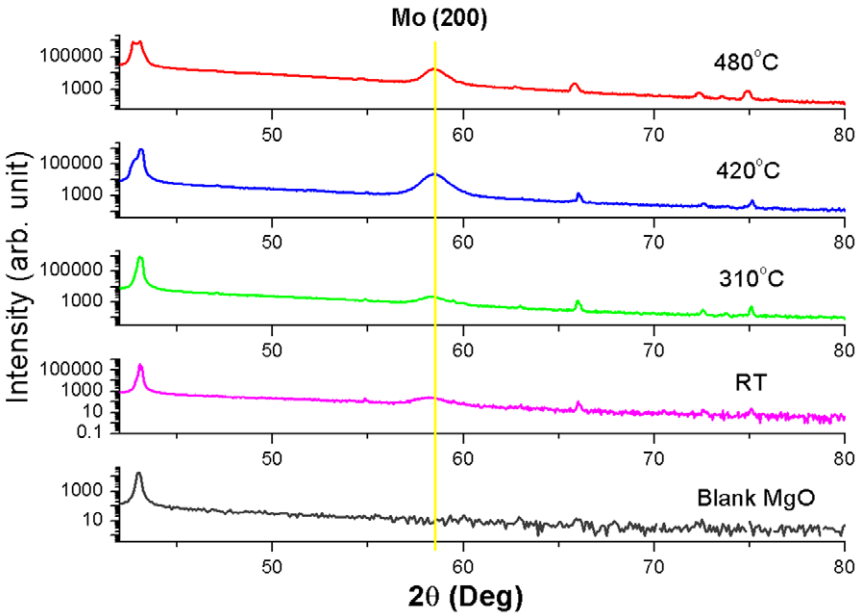

Figure 18. X-ray θ-2θ diffraction characterization of Mo layers grown on MgO substrates at RT but annealed at different temperatures. A major Mo(200) peak is established by ~420 °C.

a power >75 W is used, Ormostamp pillars with relatively high aspect-ratio were created and the resultant imprinting process was not efficient due to the plastic nature of Ormostamp (figure 16(*h*)). However, this effect is not limited to Ormostamp [120] and is a feature of all high-aspect-ratio pillar imprinting.

In NIL practice, a successful demolding process is the final key factor for obtaining high-quality patterns. This raises another issue with Ormostamp involving appropriate adhesive property of the three key interfaces: (1) good adhesion between Ormostamp and its host substrate (e.g. PET); this is achieved by the adhesion promoter—Ormoprime08; (2) good adhesion between resist and substrate (e.g. single-crystal oxides); this can be optimized by thorough surface cleaning and hydrophilic treatment of the substrate; and (3) low adhesion between Ormostamp and resist; this is achieved by coating the release layer, trichloro(1H,1H,2H,2H-perfluorooctyl)silane, on the Ormostamp. All the three interfaces are critical for a good demolding process. By selectively eliminating good adhesive qualities of (1) or (2), we observed that either the resist peels-off and sticks to the Ormostamp (figure 17(*a*)), or the Ormostamp peels off and sticks to the resist (figure 17(*b*)). Both these scenarios should be avoided in the demolding process. A thorough cleaning of both the stamp host and the substrate is recommended. For some materials with good water absorption properties, long time baking, and/or UV-Ozone and/or low-power oxygen plasma etching might be necessary. Large area nanostructures can be obtained after resolving the demolding issues, as illustrated in figure 17(*c*).

2.4.4. Crystallization of Mo mask. For epitaxial patterning it is also important to optimize the Mo mask that is widely used due to its high melting point and convenient liftoff. It has been experimentally found that Mo tends to crystallize on single crystal substrates, such as on MgO or $SrTiO_3$, before it reaches its melting point. Such crystallization may or may not hinder its subsequent liftoff process, depending on the different crystallization orientations [121]. Guilloux-Viry *et al* showed that Mo can grow epitaxially along (200) on MgO(100) at a substrate temperature above 450 °C [122]. For mask application, Mo is deposited at room temperature but heated to elevated temperatures for epitaxial growth. Mo thin films, deposited on MgO at room temperature but post-annealed at different high temperatures (figure 18), showed the onset of a Mo(200) peak in x-ray θ-2θ scans, indicating that Mo tends to crystallize along (200) on MgO substrate upon annealing. Such crystallization is initiated at ~310 °C and is fully established at ~420 °C. However, this crystallization—along (200)—does not seem to affect the subsequent liftoff process. On the other hand, similar crystallization effect along a different orientation, Mo(110), deposited on $SrTiO_3$ substrate affect the liftoff as reported by Suzuki *et al*. To solve this problem, a Mo/SiO_x bilayer resist was used to avoid the Mo crystallization by simply depositing the amorphous SiO_x at the bottom (figure 19) [121].

2.4.5. Reliable liftoff through mask undercutting. In any resist-based lithography techniques, the liftoff step plays a most important role in determining the quality of the final patterned structures. For single nanostructure devices made by AFM-lithography or EBL, the quality of the final patterns can be examined by *in-situ* AFM or SEM imaging. However, the process is time-consuming for large-area, parallel patterning techniques such as NIL. Therefore, a predictable and reliable liftoff process that yields high-quality patterns becomes particularly important for techniques such as NIL.

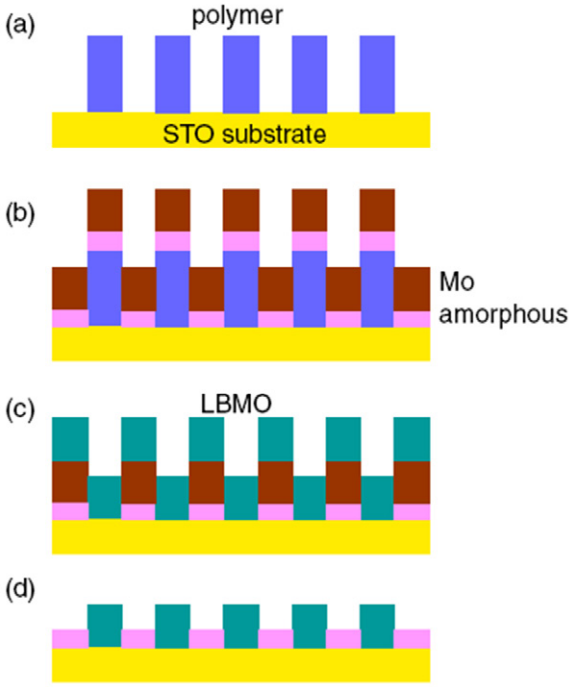

Figure 19. Schematic figure of the process flow of the modified NIL-Mo liftoff technique at high temperature: (*a*) fabricating polymer pattern on $SrTiO_3$ substrate by NIL, (*b*) depositing Mo and amorphous layer on polymer pattern and removing polymer pattern with remover, (*c*) depositing $La_{0.8}Ba_{0.2}MnO_3$ at high temperature, and (*d*) removing Mo mask and $La_{0.8}Ba_{0.2}MnO_3$ on it. Reprinted with Permission from [121]. Copyright 2009 The Japan Society of Applied Physics.

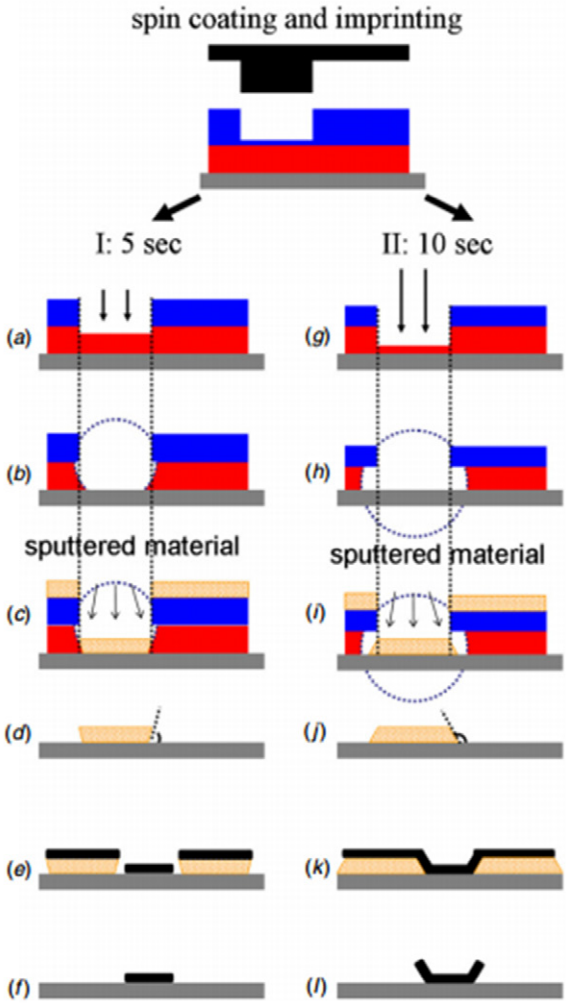

Figure 20. Illustration of NIL process for epitaxial patterning with a short (5 s) dry-etch step (*a*)–(*f*) and a conventional process with a longer (10 s) dry-etch step. The circles in (*b*) and (*h*) show the edge of isotropic removal of the polymeric sacrificial resist layer during developing. Reprinted with permission from [111]. Copyright 2011 Institute of Physics Publishing.

Single-layer resist template sometimes fails to provide a good liftoff due to the unfavorable depositions along the side-walls of the template. Such effect becomes more significant for meso- and nano-scale patterns compared with micro-scale ones. It is also a universal phenomenon observed for almost all kinds of deposition techniques, especially for those with poor directionality of the depositing flux. To overcome this issue, an additional undercut resist layer is often used (e.g. LOR resist series, MicroChem LLC). This layer is coated prior to the lithography-resist (e.g. PMMA), and then selectively developed after the lithography. The idea is to create an undercut profile of the bilayer-resist for subsequent metallization. Such undercut has proven to be efficient for liftoff [123]. In addition, the bilayer-resist also offers the possibility of varying the feature size by controlling the degree of undercutting [124].

In the epitaxial patterning process using Mo mask, two liftoff processes are required: (1) resist liftoff after deposition of Mo layer, and (2) Mo liftoff after deposition of epitaxial material layer. Suzuki *et al* used a bilayer-resist undercut for Mo mask deposition, however, the undercut of Mo mask for subsequent $Fe_{2.5}Mn_{0.5}O_4$ deposition was not described [108]. We showed that the cross-section profile of the Mo mask is also critical for the final liftoff [111]. We further demonstrated a modified process that can enable a natural undercut profile of the Mo mask (figure 20) [111, 125]. Specifically, a bilayer of polymeric undercut resist and imprint resist was thermally imprinted with an appropriate stamp. Then, a brief anisotropic de-scum etch step removes the residue of the imprint resist and a certain amount of the undercut resist (figure 20(*a*)). The undercut resist was then wet-etched appropriately to develop a wedge-shaped resist profile. Since the wet-etch proceeds in a nearly isotropic manner, the etched resist profile therefore can be approximated by a circle, with the center located at the start point of the etch (figure 20(*b*)). The Mo layer is then deposited (figure 20(*c*)), followed by the polymer-resist liftoff (figure 20(*d*)). The wedge-shaped resist produced a natural undercut profile of the Mo mask. Epitaxial material is then deposited at high temperature onto the Mo template (figure 20(*e*)), followed by the Mo liftoff in the H_2O_2 solution (figure 20(*f*)). Owing to the Mo undercut, very clean liftoff can be obtained and high quality epitaxial patterned structures can be produced. The duration of the de-scum etch step in figure 20(*a*) is the key to obtain the desired wedge-shaped polymer resist profile. Figure 20(*g*)–(*l*) illustrates a process with a de-scum etch duration increased by a factor 2. In brief, the start point of the wet-etch was moved downward, deep into the undercut

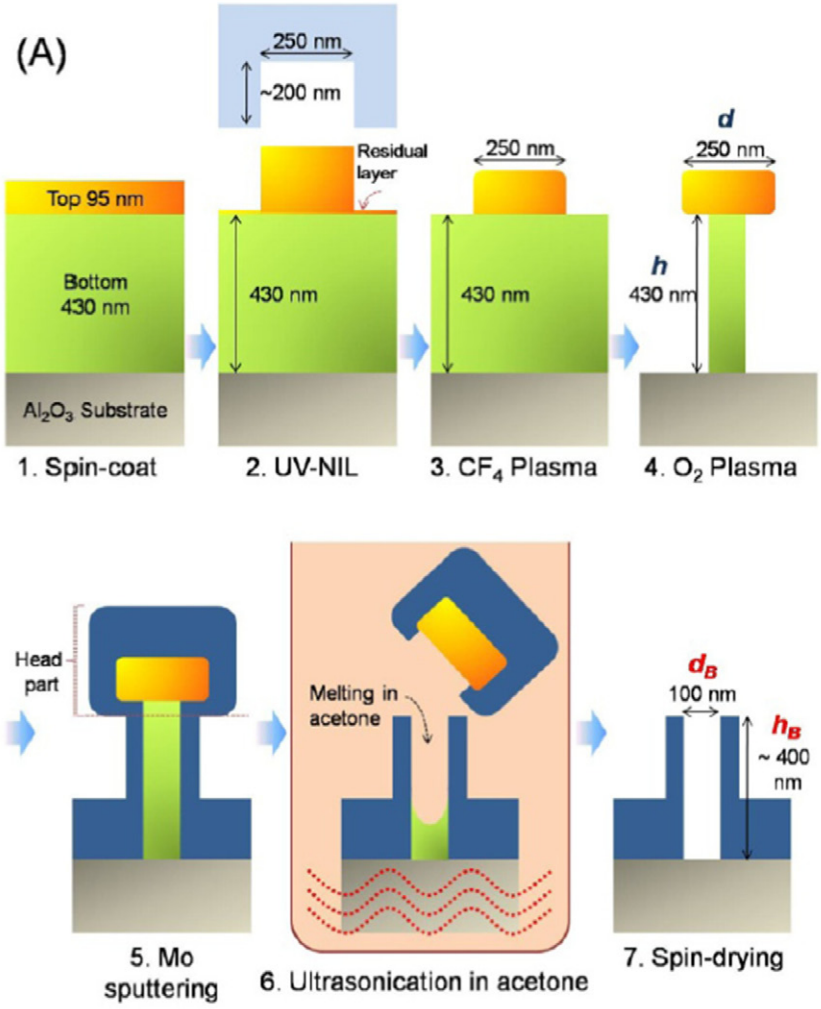

Figure 21. Schematic representation of the process involved in the fabrication of size-reducible high aspect-ratio hollow Mo nanomasks. Reprinted with permission from [129]. Copyright 2011 Institute of Physics Publishing.

resist layer by the longer anisotropic de-scum etch. After the isotropic wet-etch, as approximated by the circle, a conventional bilayer resist undercut was created, figure 20(*h*). The different resist profiles significantly affected the cross-sectional profiles of the deposited Mo structures, which further lead to a failure of liftoff.

Material deposition along the sidewall of the template is not always a nuisance that one wants to eliminate. Such deposition can be used for fine structure patterning beyond the size limit of the stamp [126–128]. For example, Cha *et al* reported a size-reducible, high-aspect-ratio, hollow Mo nanomask that was obtained from intentional side-wall deposition on the template, and demonstrated the fabrication of epitaxial 3D ferromagnetic nanostructures with high controllability [129]. The process of creating the hollow Mo mask is illustrated in figure 21. In their experiment, a bilayer resist is imprinted by a stamp with 200 nm feature size, and subsequently developed to form a typical undercut. Amorphous Mo was deposited on the patterned polymer substrate that covered all over the resist pillar (with a big head) including its sidewalls. The top head region of the pillar is then cleaved by ultrasonication. After acetone cleaning and spin-drying, a hollow Mo mask with a reduced window size ~100 nm was created for subsequent epitaxial deposition. It was noted that the size of the final structure is determined by the window size of the hollow mask, which is further controlled by the duration of the selective etching of the bottom resist layer during the undercut development. This result provided a simple method for the fabrication of integrated epitaxial nanostructure arrays with potential to overcome the present resolution limit.

2.4.6. Nanoseeding and heterostructures integration. In this section, we briefly introduce a developing technique named nanoseeding growth. It is a large-area and position-specific epitaxial growth that can be viewed as an extension of NIL-based epitaxial patterning. Different from the processes discussed so far, nanoseeding aims to fabricate nanocomposites such as ferromagnetic or ferroelectric nanodots array embedded in another function material matrix. A variety of functionalities can arise by coupling the functionalities of the nanophase and a matrix through hetero-epitaxial interfaces [130–133].

The nanoseeding process involves, as a first step, epitaxial patterning of nanoseeds in an ordered array on the

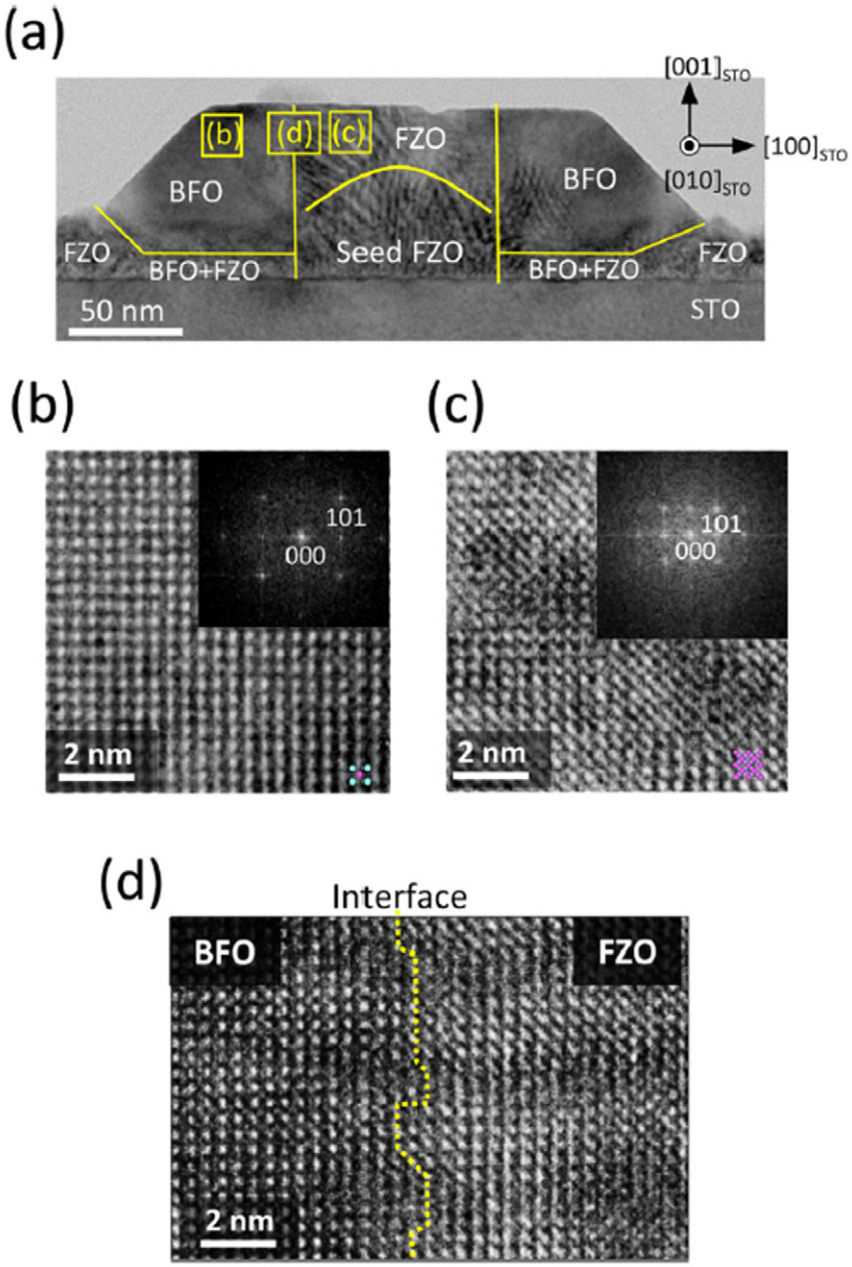

Figure 22. Cross-sectional TEM images of the (*a*) whole FZO core/BFO shell structure, (*b*) BFO shell at point '(*b*)' in figure (*a*), (*c*) FZO core grown by co-deposition at point '(*c*)', and (*d*) interface at point '(*d*)'. Reprinted with permission from [131]. Copyright 2013 AIP Publishing LLC.

substrate. This is done by NIL and Mo liftoff, combined with dry deposition of the seed material. Next, the matrix materials are deposited and they are selectively grown on the substrate surface but avoiding the nanoseeds, due to minimization of total free energy required for the formation of the interface between the two phases and the nanoseeded substrate. Applying this strategy, Sakamoto *et al* demonstrated fully aligned epitaxial $(Fe,Zn)_3O_4$ nanodots on $SrTiO_3(001)$ substrate, that were perfectly surrounded by an insulating $BiFeO_3$ matrix (figure 22). They found that a perfect selectively-growth of $BiFeO_3$ can be achieved for $(Fe,Zn)_3O_4$ small dots (<800 nm).This method was also extended to the fabrication of $(Fe,Zn)_3O_4/BiFeO_3$ core-shell type structure by using a co-deposition method [131]. As shown in figure 22, it is obvious that $BiFeO_3$ grew epitaxially along the side of the $(Fe,Zn)_3O_4$ dots, passing over the area of the $(Fe,Zn)_3O_4$ terrace and forming the shell/matrix, while $(Fe,Zn)_3O_4$ grew epitaxially on top of the $(Fe,Zn)_3O_4$ dots (seeds). In general, the nanoseeding technique achieves epitaxial fabrication of functional nanocomposites and resolves the issue of precise positional alignment of materials with high density nanostructure integration. The position alignment relies on pre-patterned nanoseed arrays, which are achieved by epitaxial patterning using NIL and Mo liftoff. This method can be extended to other material combinations and may lead to advanced

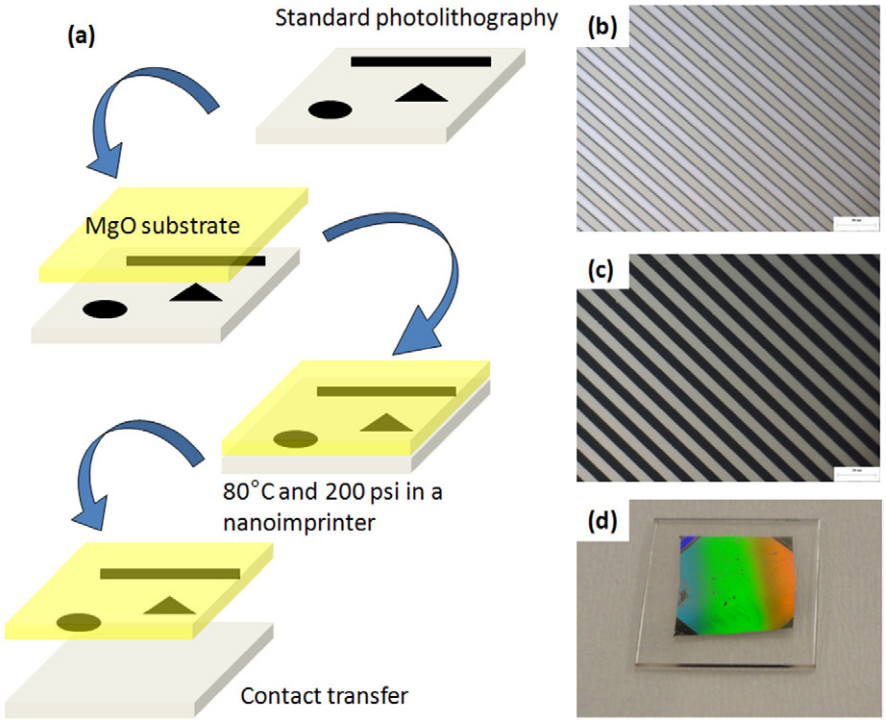

Figure 23. (*a*) Illustration of the contact-transfer process that releases the AZ1512 resist feature from a Si wafer to a MgO substrate. (*b*) Optical image of transferred AZ1512 wire pattern on MgO substrate. (*c*) Optical image of Mo wire pattern on MgO substrate after mask transfer. (*d*) Photograph image of epitaxial Fe wire arrays on transparent, 1 cm × 1 cm MgO substrate after deposition and Mo liftoff.

integration of hetero-junctions composed of oxide materials with precise position, size and shape controllability over a large area.

2.5. Contact-transfer and structure release

In standard lithography, the micro- and nano-structures are fabricated on a certain rigid substrate (e.g. Si wafer) and are bound to the substrate permanently. This rigidness impedes the fabrication and incorporation of micro- and nano-devices on flexible substrates, which is a critical step toward future soft-electronics [134–138]. Besides, it is difficult to translate the favorable economic scaling to industrial manufacturing since the wafer volume is still comparatively small. To solve the above issues, a roll-to-roll process has been developed that can achieve patterned nanostructures directly on flexible substrate with high-throughput and high-speed [139]. However, certain materials and mature devices are incompatible with the roll-to-roll process. An alternative approach is therefore to fabricate the structures on conventional substrate using standard lithography, but then transport the products to another substrate using contact-transfer. The transferred objects can be preliminary resist patterns, intermediate device components, or mature devices [140].

Contact-transfer can enable epitaxial patterning in such a way that it allows transfer of resist patterns to 'hard-to-tackle' substrates, such as ones with very small dimension, irregular shape, non-flat surface, and/or very thin/soft material, where the conventional spin-coating is unachievable. Cheng *et al* demonstrated transfer bonding of PMMA resist from NIL stamps to both flat and pre-patterned substrates, using a technique call reverse imprinting [141–143]. Furthermore, additional resist layers can be continuously piled up to form 3D polymer structures. In some cases such transfer bonding can be made easier under elevated temperatures and/or pressures. In this sense, a typical nanoimprinter, being a temperature and pressure source, serves a good platform for such transfer bonding process. For example, we used a nanoimprinter (Nanonex NXB-100) and demonstrated successful transfer bonding of AZ1512 photoresist from Si wafer to MgO substrate for epitaxial patterning (figure 23(*a*)). To reduce the adhesion between the photoresist and the Si wafer, we directly spin-coated AZ1512 on clean Si/SiO_2 surface without the HDMS evaporation. The MgO(001) substrate was pre-cleaned and baked on a hotplate at 200 °C for 10 min to remove the absorbed water. Micrometer AZ1512 wire array were directly transferred onto MgO substrates for subsequent metallization (figure 23(*b*)). The resist transfer process was done in a nanoimprinter, which provides the ideal pressure and temperature environment (200 psi and 80 °C) needed for the transfer. For epitaxial patterning, the AZ1512 mask was then transferred to Mo mask (figure 23(*c*)). Finally, figure 23(*d*) shows a photograph of the epitaxial Fe micrometer wire patterns obtained on MgO substrate using the Mo liftoff process introduced in the earlier section.

Another process related to this subject is the transfer and/or release of the epitaxially patterned structures through substrate etching [144–147]. This method allows the structures to be transported to another substrate (such as a plastic film) or their release to a free-standing form (e.g. in solution). The process enables the epitaxial structures to be incorporated in devices with more flexibility, but not bound to the original

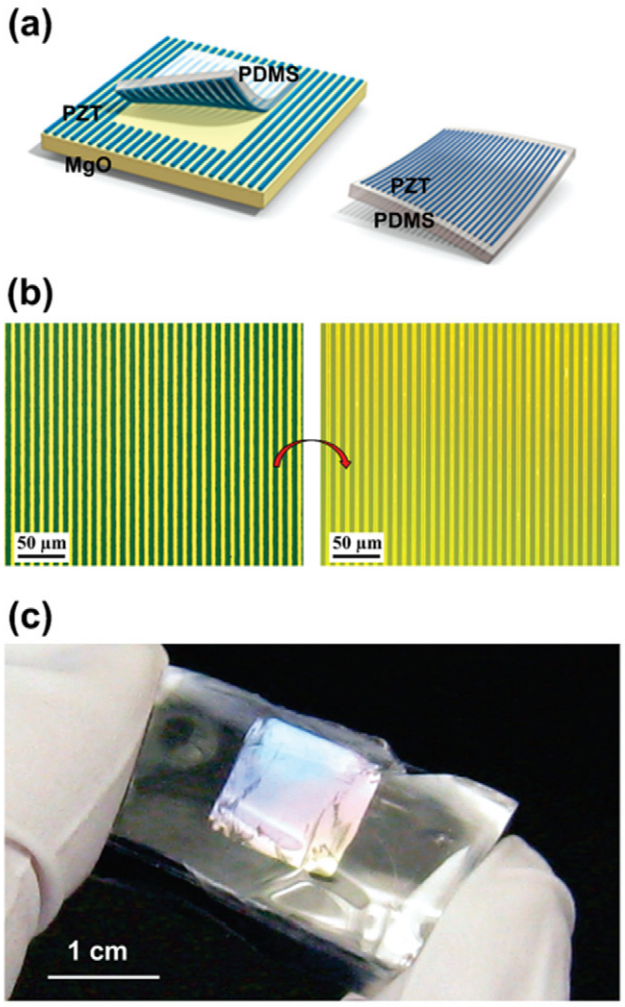

Figure 24. Transfer printing of PZT ribbons onto flexible rubber substrates. (*a*) Crystalline PZT ribbons are synthesized on an MgO host substrate, which is subsequently etched, and the ribbons are transfer printed onto flexible PDMS rubber. (*b*) Optical micrograph of PZT ribbons on MgO substrate before transfer, and PZT ribbons on PDMS after transfer printing. (*c*) Photograph of a piece of PDMS with PZT ribbons covering the top surface. Reprinted with permission from [148]. Copyright 2010 American Chemical Society.

substrate required for epitaxial growth. For example, Qi *et al* reported an approach to transfer epitaxial PZT ribbons from the host MgO substrate to PDMS rubber substrate using selective etching of MgO in 20% phosphoric acid [148]. The exposed MgO between the PZT ribbons provided an avenue for the acid to undercut and loosen the ribbons without completely dislocating them. Transfer printing of PZT ribbons was done by bringing a piece of PDMS into conformal contact with the wafer and quickly peeling it back to retrieve the ordered ribbon arrays (figure 24(*a*)). Similarly, such substrate etching can also be realized via dry etching methods such as RIE [116]. On the other hand, if the epitaxial growth does not require a specific host single-crystal substrate, the material can be simply patterned on a 'sacrificial layer' that is then selectively etched after the lithography to release the patterned structures [149–154].Such approach has been widely adopted in high-volume production of lithographically fabricated free-standing nanostructures.

3. Conclusion and perspectives

The capabilities of controlling the structural and functional properties of thin-films are being continuously developed by various physical deposition technologies. In parallel, new lithography techniques are being developed to meet the urgent need for device miniaturization. Epitaxial patterning, as a combined effort, allows the miniaturization of functional devices that incorporates thin-film components into nanoscale architectures while keeping their functional properties unmodified. In this brief review, we summarized the status of current technology for epitaxial patterning under the main scheme of 'lithography, metallization and liftoff'. Specifically, conventional EBL and AFM-lithography are good choices for single-nanostructured devices with a resolution down to tens of nanometers; however, their sequential nature impedes their application for high volume production. In order to be compatible with high-temperature deposition, metallic and ceramic resists with high melting points have been proposed to replace the conventional polymer resists. For AFM-lithography, the local-anodic-oxidation process is predominantly used to define patterned structures on the resist layer. Conventional photolithography has been demonstrated to be compatible with epitaxial patterning however it still suffers from the resolution limit dictated by the light wavelength. Nanotencil lithography, being a resist-free technique, has been widely applied for epitaxial patterning of many materials especially those that are incompatible with resist processing. It is a quite straightforward technique and incurs the least process modification as compared with epitaxial growth of continuous films. The clogging and blurring effects are two main drawbacks, limiting the highest achievable resolution for this technique. Nevertheless, sub-100 nm features have been reported by carefully minimizing the influence from both effects. Nanoimprint lithography is another parallel patterning technique which has experienced great developments in the past decade. The combination of nanoimprint and Mo-liftoff has been widely used for large-area, deep-nanoscale epitaxial patterning of various oxides and metals. As an important extension of nanoimprint lithography, nanoseeding assembly can achieve epitaxially patterned functional nanocomposites and advanced integration of hetero-structures. Contact transfer enables resist patterns and/or epitaxial patterned structures to be transported from the host to new substrates, usually flexible ones on which the direct lithography are often difficult to perform. In addition, by using selective substrate etching (dry or wet), the epitaxial structures can be released with complete freedom. Finally, new lithography techniques, such as the block-copolymer lithography, are being developed to push the resolution limit down to several nanometers. They are expected to come across novel nanoscale functional properties of epitaxial materials, yielding new desire for epitaxial patterning processes with improved resolution and enhanced precision.

Acknowledgements

WZ is very grateful for the early mentorship on lithography from Dr Dirk Weiss. WZ would like to thank Dr Weilun Chao and Dr Deirdre Olynick for their hospitality during his stay at the Molecular Foundry, Berkeley. We thank Professor Karl Bohringer, Dr Yufeng Hou and Zheng Li for insightful discussions. This work was supported by NSF–DMR under grant #1063489. We also acknowledge use of the UW Microfabrication Facility, a member of the National Nanotechnology Infrastructure Network.

References

[1] Martin L W *et al* 2010 *Mater. Sci. Eng.*: R. **68** 89
[2] Ramesh R *et al* 2007 *Nat. Mater.* **6** 21
[3] Opel M *et al* 2012 *J. Phys. D: Appl. Phys*. **45** 033001
[4] Arora H *et al* 2010 *Science* **330** 214
[5] Ganpule C S *et al* 1999 *Appl. Phys. Lett*. **75** 409
[6] Takamura Y *et al* 2006 *Nano Lett*. **6** 1287
[7] Folven E *et al* 2012 *Nano Lett*. **12** 2386
[8] Paz E *et al* 2010 *Nanotechnology* **21** 255301
[9] Ciria M *et al* 2009 *Phys. Rev.* B **80** 094417
[10] McMorran B J *et al* 2010 *J. Appl. Phys*. **107** 09D305
[11] Roshchupkina O D *et al* 2012 *J. Appl. Phys*. **112** 033901
[12] Reagor D W *et al* 2005 *Nat. Mater*. **4** 593
[13] Aurino P P *et al* 2013 *Appl. Phys. Lett*. **102** 201610
[14] Martin J I *et al* 2003 *J. Magn. Magn. Mater*. **256** 449
[15] Adeyeye A O and Singh N 2008 *J. Phys. D: Appl. Phys*. **41** 153001
[16] Lau J W and Shaw J M 2011 *J. Phys. D: Appl. Phys*. **44** 303001
[17] Yu Z Q *et al* 2007 *Nanotechnology* **18** 115601
[18] Zabaleta J *et al* 2012 *J. Appl. Phys*. **111** 024307
[19] Das R *et al* 2012 *J. Appl. Phys*. **111** 104115
[20] Banerjee N *et al* 2013 *J. Alloy Compounds* **547** 147
[21] Cummings K D *et al* 1989 *J. Vac. Sci. Technol.* B **7** 1536
[22] Satyalakshmi K M *et al* 2000 *J. Vac. Sci. Technol.* B **18** 3122
[23] Samantaray C B *et al* 2008 *J. Vac. Sci. Technol.* B **26** 2300
[24] Mohamed K *et al* 2009 *Microelectron. Eng*. **86** 535
[25] Mohamed K *et al* 2013 *Nanotechnology* **24** 015302
[26] Muhammad M *et al* 2011 *J. Vac. Sci. Technol.* B **29** 06F304
[27] Salerno M *et al* 2007 *J. Micromech. Microeng*. **17** 2414
[28] Myers B D *et al* 2006 *Nano Lett.* **6** 963
[29] Joo J *et al* 2006 *Nano Lett*. **6** 2021
[30] Banerjee N *et al* 2012 *Appl. Phys. Lett*. **100** 041601
[31] Banerjee N *et al* 2013 *Appl. Phys. Lett*. **102** 142909
[32] Xie X *et al* 2006 *Mater. Eng.* R **54** 1
[33] Tseng A A *et al* 2005 *J. Vac. Sci. Technol.* B **23** 877
[34] Tseng A A 2011 *Small* **7** 3409
[35] Day H C *et al* 1993 *Appl. Phys. Lett*. **62** 2691
[36] Campbell P M *et al* 1995 *Appl. Phys. Lett*. **66** 1388
[37] Snow E S *et al* 1995 *Appl. Phys. Lett*. **66** 1729
[38] Hirooka M *et al* 2004 *Appl. Phys. Lett*. **85** 1811
[39] Li R-W *et al* 2004 *J. Appl. Phys*. **95** 7091
[40] Pellegrino L *et al* 2005 *Appl. Phys. Lett*. **87** 064102
[41] Li R-W *et al* 2005 *Nanotechnology* **16** 28
[42] Schmidt T *et al* 1998 *Appl. Phys. Lett*. **73** 2173
[43] Matsumoto K *et al* 2000 *Appl. Phys. Lett*. **76** 239
[44] Bouchiat V *et al* 2001 *Appl. Phys. Lett*. **79** 123
[45] Farkas N *et al* 2004 *J. Vac. Sci. Technol.* A **22** 1879
[46] Tully D C *et al* 1999 *Adv. Mater*. **11** 314
[47] Sugimura H *et al* 2002 *Adv. Mater*. **14** 524
[48] Lee W *et al* 2002 *Langmuir* **18** 8375
[49] Ara M *et al* 2002 *Appl. Phys. Lett*. **80** 2565
[50] Hoeppener S *et al* 2006 *Adv. Funct. Mater*.**16** 76
[51] Martin-Olmos C *et al* 2012 *Adv. Funct. Mater*. **22** 1482
[52] Martin C *et al* 2005 *Nanotechnology* **16** 1016
[53] Pires D *et al* 2010 *Science* **328** 732
[54] Snow E S *et al* 1995 *Science* **270** 1639
[55] Held R *et al* 1997 *Appl. Phys. Lett*. **71** 2689
[56] Sugimura H *et al* 1994 *J. Vac. Sci. Technol.* B **12** 2884
[57] Wang D *et al* 1995 *Appl. Phys. Lett*. **67** 1295
[58] Snow E S *et al* 1996 *Appl. Phys. Lett*. **69** 269
[59] Rolandi M *et al* 2002 *Adv. Mater*. **14** 191
[60] Pellegrino L *et al* 2006 *Adv. Mater*. **18** 3099
[61] Suzuki N *et al* 2008 *Adv. Mater*. **20** 909
[62] Goto K *et al* 2009 *J. Appl. Phys*. **105** 064301
[63] Goto K *et al* 2009 *Nano Lett*. **9** 1962
[64] Goto K *et al* 2010 *Nano Lett*. **10** 2772
[65] Gross L *et al* 2007 *Appl. Phys. Lett*. **90** 093121
[66] Savu V *et al* 2008 *J. Vac. Sci. Technol.* B **26** 2054
[67] Zahl P *et al* 2005 *Rev. Sci. Instrum*. **76** 023707
[68] Grevin B *et al* 2011 *Rev. Sci. Instrum*. **82** 063706
[69] Grevin B *et al* 2013 *J. Vac. Sci. Technol.* B **31** 021803
[70] Guo H *et al* 2008 *Rev. Sci. Instrum*. **79** 103904
[71] Wasserman J L *et al* 2008 *Rev. Sci. Instrum*. **79** 073909
[72] You S *et al* 2010 *Small* **6** 2146
[73] Blech V *et al* 2006 *J. Vac. Sci. Technol.* B **24** 55
[74] Lee W *et al* 2008 *Nat. Nanotechnol.* **3** 402
[75] Gao X *et al* 2009 *Adv. Funct. Mater*. **19** 3450
[76] Vrejoiu I *et al* 2008 *Adv. Funct. Mater*. **18** 3892
[77] Lu X *et al* 2011 *Nano Lett*. **11** 3202
[78] Pereira A *et al* 2008 *Small* **4** 572
[79] Aksu S *et al* 2010 *Nano Lett*. **10** 2511
[80] Bates J R *et al* 2013 *Nanotechnology* **24** 115301
[81] Fernandez-Cuesta I *et al* 2006 *J. Vac. Sci. Technol.* B **24** 2988
[82] Fernandez-Cuesta I *et al* 2005 *Nanotechnology* **16** 2731
[83] Takano N *et al* 2006 *J. Micromech. Microeng*. **16** 1606
[84] Vazquez-Mena O *et al* 2008 *Microelectron. Eng*. **85** 1237
[85] Yan X M *et al* 2005 *Nano Lett*. **5** 1129
[86] Vazquez-Mena O *et al* 2009 *Nanotechnology* **20** 415303
[87] te Riele P *et al* 2007 *J. Phys.: Conf. Ser*. **59** 404
[88] Linklater A *et al* 2008 *Nanotechnology* **19** 285302
[89] Shin H J *et al* 2005 *Appl. Phys. Lett*. **87** 113114
[90] Cojocaru C-V *et al* 2005 *Appl. Phys. Lett*. **86** 183107
[91] Cojocaru C -V *et al* 2006 *IEEE. Trans. Nanotechnol*. **5** 470
[92] Cojocaru C-V *et al* 2010 *Appl. Surf. Sci*. **256** 4777
[93] Morelli A *et al* 2013 *J. Appl. Phys*. **113** 154101
[94] Liu H J *et al* 2006 *J. Appl. Phys*. **100** 014306
[95] Wen T L *et al* 2012 *Nano. Lett*. **12** 5873
[96] Nechache R *et al* 2011 *Adv. Mater*. **23** 1724
[97] Nechache R *et al* 2012 *J. Phys.: Condens. Matter*. **24** 142202
[98] Nechache R *et al* 2012 *J. Solid. State. Chem*. **189** 13
[99] Vrejoiu I *et al* 2011 *Nano Rev.* **2** 7364
[100] Chou S Y *et al* 1995 *Appl. Phys. Lett*. **67** 3114
[101] Chou S Y *et al* 1996 *Science* **272** 85
[102] Guo L J 2007 *Adv. Mater*. **19** 495
[103] Costner E A *et al* 2009 *Annu. Rev. Mater. Res*. **39** 155
[104] Guo L J 2004 *J. Phys. D: Appl. Phys*. **37** R123
[105] Schift H 2008 *J. Vac. Sci. Technol.* B **26** 458
[106] Lan H *et al* 2013 *J. Nanosci. Nanotechnol.* **13** 3145
[107] Lan H *et al* 2007 *Microelectron. Eng*. **84** 684
[108] Suzuki N *et al* 2008 *Small* **4** 1661
[109] Yamanaka S *et al* 2009 *Solid State Commun*. **149** 729
[110] Yamanaka S *et al* 2010 *Nano Lett*. **11** 343
[111] Zhang W *et al* 2011 *J. Micromech. Microeng*. **21** 045024
[112] Rolland J P *et al* 2004 *Angew. Chem. Int. Ed*. **43** 5796
[113] Khang D-Y *et al* 2004 *Langmuir* **20** 2445
[114] Barbero D R *et al* 2007 *Adv. Funct. Mater*. **17** 2419
[115] Weiss D N *et al* 2010 *J. Vac. Sci. Technol.* B **28** 823
[116] Zhang W *et al* 2012 *J. Appl. Phys*. **111** 07B509
[117] Muhlberger M *et al* 2009 *Microelectron. Eng*. **86** 691
[118] Klukowska A *et al* 2009 *Microelectron. Eng*. **86** 697
[119] Schift H *et al* 2009 *J. Vac. Sci. Technol.* B **27** 2846

[120] Finn A *et al* 2013 *Microelectron. Eng*. **110** 112
[121] Suzuki N *et al* 2009 *Jpn. J. Appl. Phys.***48** 116511
[122] Guilloux-Viry M *et al* 1996 *Thin Solid Films* **280** 76
[123] Zhang W *et al* 2010 *J. Appl. Phys*. **107** 09D724
[124] Hu W *et al* 2007 *J. Vac. Sci. Technol.* A **25** 1294
[125] Zhang W *et al* 2013 *J. Appl. Phys*. **113** 17B502
[126] Hattori A N *et al* 2011 *Nanotechnology* **22** 415301
[127] Kushizaki T *et al* 2012 *Nanotechnology* **23** 485308
[128] Takami H *et al* 2012 *Appl. Phys. Lett* **101** 263111
[129] Cha N G *et al* 2011 *Nanotechnology* **22** 185306
[130] Sakamoto T *et al* 2012 *Nanotechnology* **23** 335302
[131] Sakamoto T *et al* 2013 *J. Appl. Phys*. **113** 104302
[132] Okada K *et al* 2013 *J. Appl. Phys*. **113** 064317
[133] Okada K *et al* 2012 *J. Appl. Phys*. **112** 024320
[134] Rogers J A *et al* 2010 *Science* **327** 1603
[135] Kim D H *et al* 2011 *Science* **333** 838
[136] Kim D H *et al* 2008 *Science* **320** 507
[137] Sekitani T *et al* 2010 *Nat. Mater*. **9** 1015
[138] Kaltenbrunner M *et al* 2013 *Nature* **499** 458
[139] Ahn S H *et al* 2008 *Adv. Mater*. **20** 2044
[140] Packard C E *et al* 2010 *Adv. Mater*. **22** 1840
[141] Bao L -R *et al* 2002 *J. Vac. Sci. Technol.* B **20** 2881
[142] Huang X D *et al* 2002 *J. Vac. Sci. Technol.* B **20** 2872
[143] Park H *et al* 2007 *J. Vac. Sci. Technol.* B **25** 2325
[144] McAlpine M C *et al* 2007 *Nat. Mater*. **6** 379
[145] McAlpine M C *et al* 2005 *Proc. IEEE* **93** 1357
[146] Edhm G *et al* 2007 *Acta Mater.* **55** 6659
[147] Chang Z C *et al* 2001 *Mater. Chem. Phys.* **70** 137
[148] Qi Y *et al* 2010 *Nano Lett*. **10** 524
[149] Linder V *et al* 2005 *Small* **7** 730
[150] Kozuka H *et al* 2012 *ACS Appl. Mater. Interfaces* **4** 6415
[151] Hu W *et al* 2008 *Adv. Mater*. **20** 1479
[152] Hu W *et al* 2009 *J. Appl. Phys*. **105** 07B508
[153] Hu W *et al* 2011 *Nanotechnology* **22** 185302
[154] Joisten H *et al* 2010 *Appl. Phys. Lett*. **97** 253112